Review in Advance first posted online on April 20, 2010. (Changes may still occur before final publication online and in print.)

Microrobots for Minimally Invasive Medicine

Bradley J. Nelson,[1] Ioannis K. Kaliakatsos,[1] and Jake J. Abbott[2]

[1]Institute of Robotics and Intelligent Systems, ETH Zurich, 8092 Zurich, Switzerland; email: bnelson@ethz.ch, ikaliakatsos@ethz.ch

[2]Department of Mechanical Engineering, University of Utah, Salt Lake City, Utah 84112; email: jake.abbott@utah.edu

Annu. Rev. Biomed. Eng. 2010. 12:55–85

The *Annual Review of Biomedical Engineering* is online at bioeng.annualreviews.org

This article's doi: 10.1146/annurev-bioeng-010510-103409

1523-9829/10/0815-0055$20.00

Key Words

microrobot, minimally invasive, medical, surgical, untethered, wireless

Abstract

Microrobots have the potential to revolutionize many aspects of medicine. These untethered, wirelessly controlled and powered devices will make existing therapeutic and diagnostic procedures less invasive and will enable new procedures never before possible. The aim of this review is threefold: first, to provide a comprehensive survey of the technological state of the art in medical microrobots; second, to explore the potential impact of medical microrobots and inspire future research in this field; and third, to provide a collection of valuable information and engineering tools for the design of medical microrobots.

Contents

1. INTRODUCTION

Minimally invasive procedures are linked with a variety of patient-oriented benefits ranging from reduction of recovery time, medical complications, infection risks, and postoperative pain to increased quality of care, including preventative care (1–4). These procedures have a long, successful history, but the area has experienced two particularly significant advances in the past decade. The first is the success of Intuitive Surgical's da Vinci: a robotic, minimally invasive surgical system. The second is the steadily increasing worldwide adoption of capsule endoscopy for gastrointestinal (GI) diagnosis. Both of these developments illustrate the acceptance that a surgeon's most important skill is cognitive ability, whereas technical skills required for precision and dexterity can often be delegated to appropriate technology (5). There is a sense that surgical microrobots "are just around the corner" (6). At the small scales envisioned, microrobots have the potential to perform tasks that are currently difficult or impossible, and they will undoubtedly lead to the development of therapies not yet conceived. Although specific applications of microrobots are still in an early concept stage, the direction in which the field is heading is rapidly solidifying.

In recent years, there has been significant progress in robot-assisted colonoscopy (7) and in miniature robots for use in the GI tract. Motivated by the capsule endoscopes already in clinical use, researchers have explored a number of technologies to expand the capabilities of these devices, ranging from lab-on-a-chip devices equipped with pressure, pH, and temperature sensors to the addition of legs and other mechanisms for controlled locomotion (see Reference 8 for a recent review). The size of these devices approaches a few centimeters, capitalizing on the relatively large size of the GI tract. However, if we were able to create microrobots with a maximum dimension of only a few millimeters or less, additional locations in the human body would become available for

wireless intervention, including the circulatory system, the urinary system, and the central nervous system. Microrobots could navigate natural pathways, enabling intervention with minimal trauma.

As we scale robots down to the microscale, the fundamental physics governing the devices remains the same, but the relative importance of physical effects changes (9, 10). Fluid viscosity and surface effects such as electrostatics dominate over volumetric effects such as weight and inertia, and the generation and storage of power becomes difficult. These challenges place strong constraints on the development of medical microrobots. In traditional robotics, one generally compartmentalizes aspects of robot design such as kinematics, power, and control. It is unlikely that miniature devices that carry small electric motors and batteries can be effectively scaled to submillimeter sizes. In the design of wireless microrobots, fabrication is fundamentally limited by scaling issues, and power and control are often inextricably linked. This forces us to take a different perspective on microrobot design than that found in traditional robotics. Engineers must give up intuition gained from designing in the macroscale world and instead rely on analysis and simulation in microrobot design. Even then, only experimental results will demonstrate the efficacy of a given microrobot design, as the world experienced by the microrobot may be difficult to model accurately.

DOF: degrees of freedom

MEMS: microelectromechanical systems

The world of a medical microrobot consists of fluid-filled lumens (i.e., tubes) and cavities, as well as soft tissues. Medical microrobots must be designed specifically to work in these environments, but the relative changes in the size, geometry, and material properties of the environment within a given procedure present design challenges. Consider, for example, a microrobot designed to work in the urinary system. The microrobot would be inserted into the urethra and would travel along this lumen to reach the bladder. If the goal is to reach a kidney, the microrobot must first navigate the bladder, which appears as a relatively large open cavity to the microrobot. To reach the kidney, the microrobot must enter the ureter, which is a lumen that enters the bladder at an oblique angle, and then navigate to the kidney. Designing a single microrobot that is able to negotiate these changing environments is not trivial. Fluid flow in the microrobot's environment also presents a significant design challenge. Consider a microrobot designed to work in the circulatory system. In addition to dealing with varying blood-vessel diameter, the microrobot must compete against the pulsating flow of blood, which is significant to a small, untethered device. Although designing functional medical microrobots is challenging from an engineering perspective, the potential rewards are vast. Wireless microrobots are an alternative to catheter-based approaches (11), but they have fundamentally different engineering-design challenges. Tethered devices cannot act as permanent or temporary implants, and their maneuverability is limited once they reach the site of interest because some degrees of freedom (DOF) are no longer available for maneuverability. Furthermore, many internal locations of the body are either inaccessible or hard to reach in a tethered fashion.

In this review, we present the state of the art in medical microrobots and discuss potential applications for these devices that are realistic for the near future. There exist surveys of the use of robotics in surgery (12, 13), but this is the first to consider microrobots in medicine. We first discuss potential microrobot functions, as well as locations in the body where microrobots are likely to perform these functions. We then discuss the critical issue of wireless power and the methods of transducing that power into locomotion. Finally, we discuss localization of in vivo microrobots, which will be required for both feedback control and safety concerns.

We will not place emphasis on wireless microelectromechanical systems (MEMS) devices, which tend to be either sensor or actuator oriented and have no locomotion capabilities (e.g., implants). An extensive discussion about BioMEMS can be found in Reference 14. Clearly, MEMS devices have the potential to be incorporated into medical microrobots. We will also not discuss medical nanorobots, which are significantly smaller than microrobots and typically envisioned as

devices to target individual cells (15, 16). Many proposed nanorobots are more like pharmaceuticals than machines, utilizing concepts from synthetic biology and requiring large numbers of them to complete a task. Some researchers are pursuing electromechanical approaches to nanorobot design, but they are still developing and characterizing the fundamental building blocks of future nanorobotic devices and are not yet ready to fabricate a nanorobot capable of performing even a simple medical task (17).

2. POTENTIAL IMPACT OF MEDICAL MICROROBOTS

2.1. Basic Functions

As the state of the art advances, we can imagine microrobots capable of carrying out complex sequences of operations, potentially autonomously. However, true microrobots will likely carry out relatively simple functions, in many cases supervised or directly teleoperated by a clinician. This will be true in the near term because of the current state of the art in technology; also, the scaling of physical effects will make the downscaling of certain technologies fundamentally infeasible. In the following, we provide a classification of simple medical microrobot tasks (**Figure 1**). Certain tasks require very simple structures, making them feasible near-term goals. As technology improves, more complex microrobots can be created to address combinations of these simple tasks (25).

2.1.1. Targeted therapy. Microrobots can be used for the localized delivery of chemical and biological substances, as well as various forms of energy. The following are some therapeutic uses for microrobots:

- Targeted drug delivery can be used to simultaneously increase the concentration of drug in a region of interest and reduce the risk of side effects in the rest of the body. The term targeted drug delivery is sometimes used to refer to therapies that target specific cells or genes, but we use the term here to refer to the targeting of a specific location in the body.
- Brachytherapy is the placement of a radioactive source, sometimes referred to as a radioactive seed, near unwanted cells such as a tumor (26). The radiated energy results in death of the cells close to the radioactive source.

Figure 1

Medical tasks for microrobots, including targeted therapy, material removal, controllable structures, and telemetry. (*a*) Targeted drug delivery will enable increased effectiveness of therapies while minimizing side effects. This microrobot, for example, is docked to a blood vessel as a proposed therapy for retinal vein occlusions (18). (*b*) Microrobots can aid in brachytherapy by carrying radioactive seeds to destroy tumors. (*c*) Time-varying magnetic fields induce heating in a microrobot, which can be used for hyperthermia therapy (19, 20). Image courtesy of Kazushi Ishiyama, Tohoku University. (*d*) In vitro stem-cell research is progressing rapidly, and microrobots can provide a method that applies these results in vivo. (*e*) Microrobots can perform ablation to remove unwanted tissue. (*f*) Microrobots can obtain tissue samples for biopsy, using mechanisms such as this device designed for a miniature endoscopic robot (21). Image courtesy of Dong-il Cho, Seoul National University. (*g*) Microrobots can act as support scaffolding for tissue-engineering applications. This image shows a construct that consists of mineralized ingrowth into a polymer scaffolding (22). Image courtesy of Arthur Sakellariou, Australian National University. (*h*) Microrobots can act as stents that can be used to keep passages open. (*i*) Microrobots can act as occlusions in cases where a passage needs to be blocked. Image courtesy of AGA Medical Corp. (*j*) Microrobots can carry or act as electrode implants in the brain. Image courtesy of Cyberkinetics Neurotechnology Systems, Inc. (*k*) Microrobots can perform wireless remote sensing, such as this intraocular oxygen sensor whose luminescence is a function of oxygen concentration (23). (*l*) A microrobot transmitting its own location is useful for localization, as well as for marking pathologies of interest. In this proposed example, a microrobot equipped with a mechanical structure capable of vibrating at ultrasonic frequencies can be localized in the body using receivers placed on the outside of the body (24).

- Hyperthermia and thermoablation refer to the local delivery of heat energy to destroy unwanted cells (27). Hyperthermia involves moderately raising temperature for extended periods of time, typically to the range of 40–45°C, to improve the effectiveness of other therapies; thermoablation involves raising the temperature to the point of cell death, which is typically above 50°C (28). The most promising methods for wireless heat delivery include high-frequency magnetic fields (27) and ultrasonic-resonating mechanical structures.

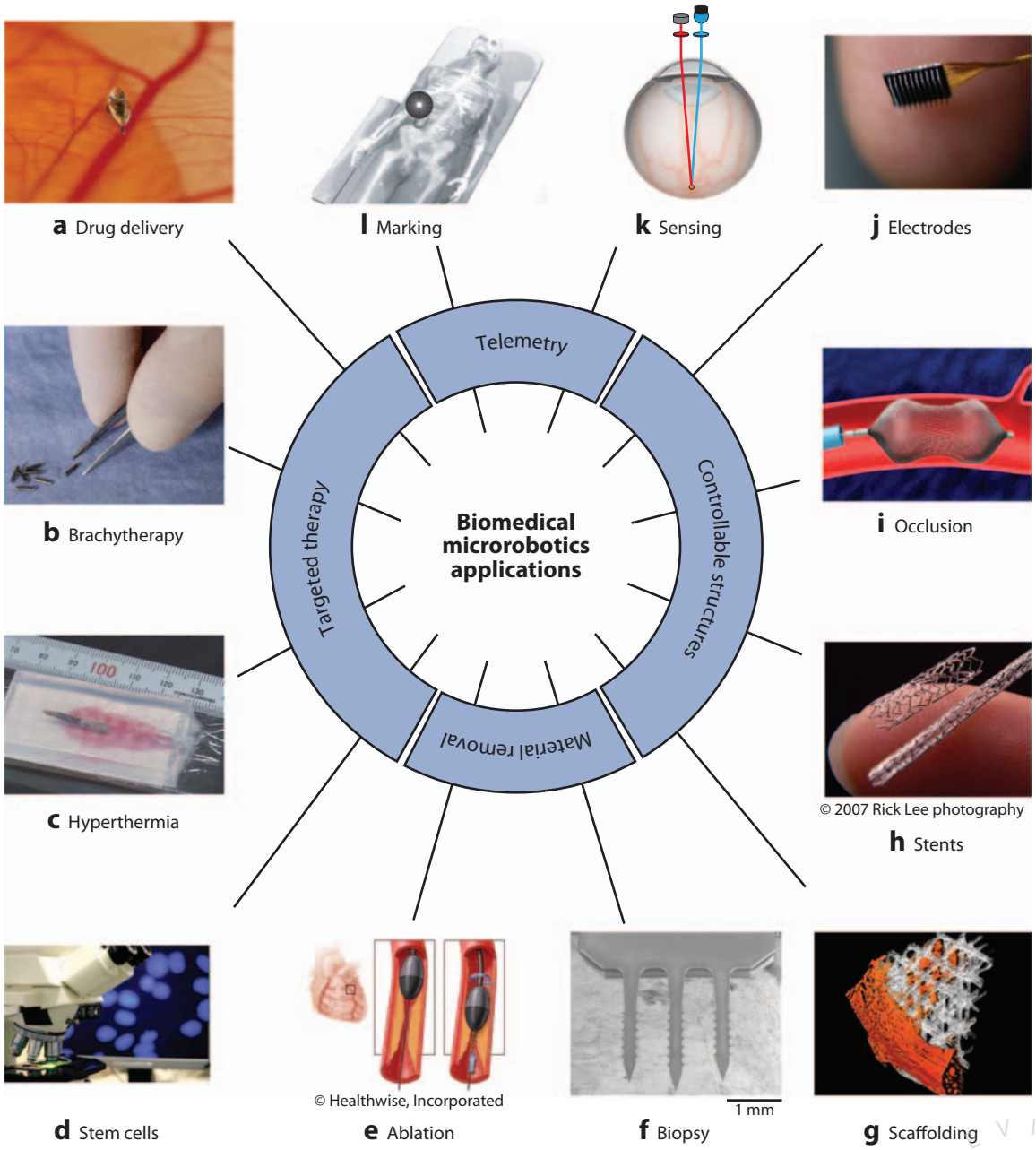

- Stem cells hold enormous potential for future therapies (e.g., regeneration of lost hearing and sight). It is not yet clear how differentiated stem cells will be implanted and fostered in vivo in a clinical setting. This may be a task well suited to microrobotic assistance.

2.1.2. Material removal. Microrobots can be used to remove material by mechanical means. If the microrobot is relatively large, it may be possible to design specialized tools to accomplish the task. However, for smaller microrobots, the microrobot itself will be the tool. The following are two methods of material removal that can be performed by microrobots:

- Ablation is the removal of material from the surface of an object. In its simplest form, this is accomplished by scraping. As we will show, microrobots may be particularly well suited for utilizing rotary motion to perform ablation tasks, which would be useful, for example, in the removal of fatty deposits from the internal walls of blood vessels. Another possibility is ultrasound ablation, in which a microrobot uses a resonating mechanical structure to emit ultrasonic pressure waves to destroy an object such as a kidney stone.
- Biopsy/excision can also be performed by microrobots. In the simplest case, the microrobot retrieves a tissue sample and is removed from the body, and the analysis is conducted ex vivo. If biopsy or excision is combined with remote-sensing technology, the sample can be analyzed in situ.

2.1.3. Controllable structures. Microrobots can act as simple static structures whose positions are controllable:

- Scaffolds act as cell support frames on which nerves can be regenerated, artificial organs developed, and blood vessels regrown. The microrobot itself can act as the scaffold, or the microrobot can deploy microscopic building blocks that act as scaffolding (29).
- Stents are structures that are used to keep passageways open. A typical example is the use of a stent to keep blood flowing though a clogged vessel. The microrobot itself would serve as the stent and would navigate and deploy in the location of interest.
- Occlusions can be introduced to intentionally block a passageway, either temporarily or permanently. Microrobots can function as occlusions, for example, to clog a blood vessel that nourishes a tumor.
- Implants/electrodes can be introduced by microrobots. A microrobot can act as a temporary or permanent implant, such as an electrode for brain stimulation. The electrode may operate wirelessly, or a wirelessly guided microrobot may tow a fine wire.

2.1.4. Telemetry. Microrobots can be used to transmit, from a specific location, information that would otherwise be difficult or impossible to obtain. This information can be transduced using a variety of methods (e.g., radio, visible light, ultrasound). Telemetry applications include remote sensing and marking:

- Microrobots can perform remote sensing. For example, microrobots can transmit the time history of a physical signal of interest (e.g., oxygen concentration) or transmit a simple binary signal upon detecting the presence of an analyte of interest (e.g., cancer, blood).
- Marking and transmitting the microrobot's position to the outside world can prove useful. It can be used for microrobot localization, and when combined with remote sensing, it can be used to localize unknown internal phenomena (e.g., bleeding). Marking requires not only sensing and transmitting, but also the ability of the microrobot to maintain its location at the site.

2.2. Application Areas

Once equipped with some basic functionalities and miniaturized to a size of a few millimeters or less, microrobots have the potential to perform medical procedures throughout the body.

MRI: magnetic resonance imaging

2.2.1. The circulatory system. The circulatory system consists of the heart and the vessels used to carry blood around the body. Blood vessels consist mainly of four types of tissue: endothelium (internal wall lining), elastic tissue (for pulsation damping), smooth muscle, and connective tissue. The relative composition of a given vessel depends on its function and distance from the heart. As the distance between the heart and a given blood vessel increases, the pressure pulsation resulting from the beating heart becomes attenuated, reaching a limiting behavior of constant flow in the capillaries.

Figure 2 shows the blood-flow velocity and Reynolds number as a function of vessel size. The Reynolds number reported is that describing pipe flow. In addition to average values, the maximum flow velocities and Reynolds numbers are also critical, reaching $Re = 8500$ in the aorta and 1000 in the arteries (30). Blood consists largely of a watery fluid named plasma, in which red and white blood cells measuring 5–10 μm and smaller platelets are suspended. Although blood has many properties (density 1060 kg m^{-3}, pH 7.38–7.42, surface tension 55–61 $\times$ 10^{-3} N m^{-1}) that are approximately the same as water, its apparent viscosity (3.5 $\times$ 10^{-3} Pa s) is three times higher, primarily owing to suspended red blood cells (30, 31). The reported properties of blood come from studies that treat it as a homogeneous fluid—an assumption that loses accuracy at the microscale. Depending on its size, a microrobot could very well experience a working environment closer to obstacle-filled plasma than "blood" as described by a homogeneous model.

Nearly every site of the body can be accessed by blood, so the circulatory system is arguably the most important application area for wireless microrobots. Some of the most promising applications for microrobots in the circulatory system include performing targeted drug delivery, removing plaque (rotational atherectomy), destroying blood clots (thrombolysis), acting as stents to maintain blood flow, acting as occlusions to intentionally starve a region of nutrition, and administering therapy for aneurysms. Microrobots could also carry electrodes for electrophysiology.

The small-diameter capillary network makes unlikely the possibility of round-trip navigation of the body, with the microrobot always moving with the flow. Consequently, a viable microrobot is likely to require the ability to move against the flow. Martel and colleagues have configured a clinical magnetic resonance imaging (MRI) system to control the movement of a magnetic bead in the circulatory system (32) and have actually performed in vivo trials in the artery of a living swine (33). They find that generating enough force to move against blood flow is challenging but possible.

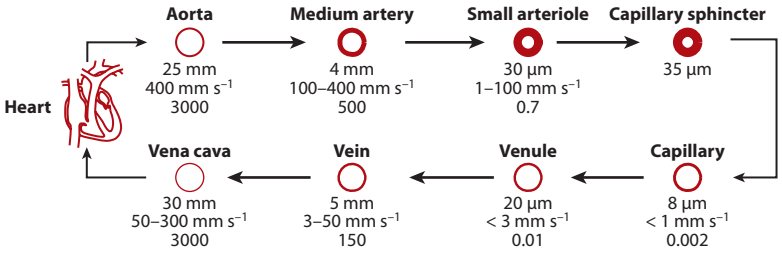

Figure 2

Schematic representation of the vessels of the cardiovascular system, with the inner diameter, average blood-flow speed, and Reynolds number from Berger et al. (30).

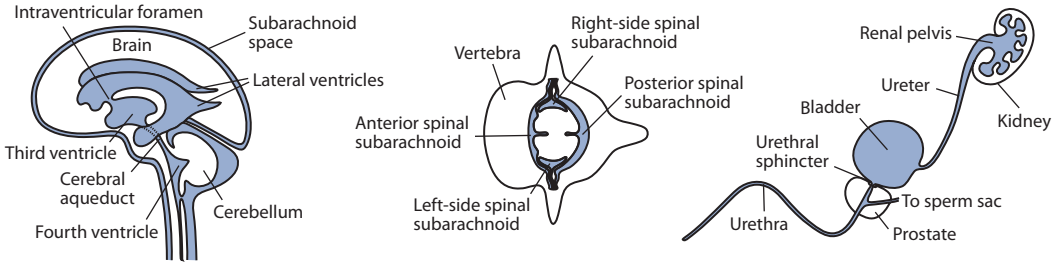

Figure 3

The central nervous system, consisting of the brain and spinal column, and the urinary system.

2.2.2. The central nervous system. The central nervous system consists of the brain, the spinal cord, and the cerebrospinal fluid in which both the brain and spine are bathed (**Figure 3**). The fluid is colorless and has properties similar to water (relative viscosity 1.020–1.027, density 1.0032–1.0048 kg m^{-3}, pH 7.35–7.7, surface tension 60–63 $\times$ 10^{-6} N mm^{-1}) (31, 34).

A recent experiment by Zaaroor et al. focused on the determination of the geometry and dimensions of the spinal subarachnoid space to provide design constraints for endoscopic visualization of the spinal canal (35). We can utilize their results to obtain design constraints for microrobots. The subarachnoid space tends to be symmetrical on the left and right sides of the spinal cord, and the anterior and posterior segments are highly asymmetrical. It may be difficult to access the anterior space in practice. A microrobot designed to fit through a 2.5-mm channel could navigate the side or posterior subarachnoid spaces in approximately 50% of the population, whereas a device designed to fit through a 1.5-mm channel would fit in at least 85% of the population. Gaining access to the ventricles of the brain from the spine is accomplished by passing through the cerebral aqueduct, which is a lumen with a 1.0–2.2 mm internal diameter that is 11.8–18.0 mm long (36).

Microrobots have the potential to dramatically affect cancer treatment in the central nervous system. Neural prostheses and deep-brain stimulation are other promising applications for microrobots that are wirelessly guided to hard-to-reach sites. The microrobots may even remain as implants. The brain's delicate structures demand appropriate caution in any procedure, and the impact of minimally invasive microrobotic procedures could be profound.

Conventional access to the brain is gained through a craniotomy, or a burr hole drilled through the skull. However, samples of the cerebrospinal fluid are usually taken with a lumbar puncture between the L3 and L4 vertebrae. Therefore, it may be possible to insert a microrobot at that site and navigate to the brain for intervention, leaving the skull intact. This principle of using percutaneous intraspinal navigation was recently applied in brain surgery through the use of catheters (37).

A great deal of research has dealt with wireless manipulation of magnetic seeds in the brain for the purpose of hyperthermia, and a number of prototype systems have been developed by a collaboration between the University of Virginia and the University of Washington (38–41). This research was accompanied by an experimental investigation of the forces required to move the seed within the brain (42). Kósa et al. propose a swimming microrobot for endoscopic procedures in the subarachnoid space of the spine (43). It is also possible that many of the tethered MEMS devices designed for use in neurosurgery (44) could be incorporated into a wireless microrobot.

2.2.3. The urinary system and the prostate. The urinary tract includes two kidneys; the urinary bladder; two ureters, which are lumens leading from the kidneys to the bladder; and the urethra, which leads from the bladder to the exterior of the body. Urine has a density and viscosity similar

to water (**Figure 3**). Each ureter is approximately 250 mm long with an internal diameter of 2.8–3 mm. The ureter enters the bladder's wall at an oblique angle to prevent back-flow of urine to the kidneys. The bladder is an elastic muscular sac capable of holding 500 ml of urine. The urethra is approximately 30–40 mm long in females, whereas in males it measures 180 mm (45, 46). At its narrowest point, the female urethra is 3.25 mm in diameter (47). The internal diameter of the urethra can be induced from catheter size, available in the range of 3–34 Fr, with the unit conversion 3 Fr = 1 mm. Adult males typically require catheters in the range of 8–22 Fr; adult females, in the range of 8–18 Fr. These values can be used as a guideline for urinary-tract microrobots. The prostate is a compound of glands that surround the urethra in men, located inferior to the bladder. These glands are enclosed in a capsule measuring $20 \times 40 \times 30\ \text{mm}^3$.

Microrobots have the potential to improve the treatment of kidney stones (nephrolithotomy). Recently, a study was performed on the factors that affect blood loss during percutaneous nephrolithotomy (PCNL) (48). Bleeding during PCNL results from injury to the renal vessels and is the most common complication of percutaneous renal surgery. Optimal access to the stone site has a direct effect on the outcome of the procedure. Multiple punctures of the kidney and perforations of the manifold that leads to the ureter (i.e., the renal pelvis) are associated with greater blood loss. There are also complications associated with extracorporeal shock-wave lithotripsy, including bleeding and infection (49). Edd et al. propose a microrobot that would swim up the ureter to destroy kidney stones in a process whose potential benefits would include less overall harm to the kidney and increased choice over the mechanism of stone destruction (50). It is also possible that the tethered and implanted MEMS devices designed for use in urology (51) could be incorporated into a wireless microrobot.

Another potential application for microrobots is in the treatment of prostate cancer. The current clinical techniques for prostate therapy involve needle insertion through the perineum, during which there is a significant risk of damage to the densely populated nerves nearby. An alternative approach is to gain access to the prostate through the colon. The distance that the needle must travel is smaller in this case, and the nerves are avoided, but complex maneuvers must be performed as opposed to the straight path of the perineum approach, and perforation of the colon increases the chance of infection. In either case, precise placement of a radioactive seed in brachytherapy is difficult because the prostate deforms and moves owing to the force of the needle, making the released location of the seed different from the planned location. A microrobot could carry a radioactive seed to the tumor site without causing the bulk deformations in the prostate that result from a needle. In addition, a microrobot could carry a single radioactive seed to a number of tumor locations, stopping at each site long enough to give the appropriate dosage. Microrobots also offer minimally invasive access to the prostate through the urethra. They could improve the effectiveness of prostate procedures and reduce the chances of nerve damage.

2.2.4. The eye. The vitreous humor of the eye is a viscoelastic gel that consists mostly of water (99%) but also contains hyaluronic acid and collagen fibrils that give it viscoelastic properties and make it more of a soft tissue than a fluid. Many procedures start with a vitrectomy, in which the vitreous is removed and replaced with a fluid similar to water or with an oil. In older adults, who are most likely to require retinal procedures, the vitreous in the posterior of the eye may have already been naturally replaced with a watery solution.

The retina is the location of the eye for which microrobots hold the greatest promise because its health is critical for vision yet it is not easily accessible. Retinal microsurgery requires sensitive manipulations that are constrained by the limits of human performance (52) and that require forces below the threshold of human perception (53), making retinal procedures both difficult and risky. In addition, current vitreoretinal surgical techniques typically require a vitrectomy to

gain access to the retina. Microrobots provide an alternative approach to retinal procedures. The appropriate entry/exit point for a microrobot is the durable pars plana. The microrobot must navigate to the retina at the posterior pole of the eye. It may be possible to conduct microrobotic procedures without first performing a vitrectomy because the small size of the microrobot will mitigate traction on the retina compared with larger tools. Avoiding vitrectomy would reduce the invasiveness of the procedure and potentially improve the health of the retina after the procedure by allowing it to maintain a more natural state. Microrobots may also be useful even after a vitrectomy because they have the potential to perform delicate tasks in a way that mitigates risk to the retina compared with manual and other robot-assisted techniques. The most promising applications of intraocular microrobots are therapies for retinal vein occlusions, detached retinas, and epiretinal membranes, as well as the diagnosis of retinal health. Trocars as large as 23-gauge, corresponding to a lumen diameter of 0.65 mm, can be used in the pars plana region with only topical anesthesia and with no suture requirement (54); this size specification serves as a goal for intraocular microrobots.

Yesin et al. propose a microrobot for intraocular procedures, controlled wirelessly with magnetic fields and tracked visually through the pupil (55). Ergeneman et al. propose an optical oxygen sensor for diagnosis of retinal health based on luminescence quenching (23). Dogangil et al. propose a method of targeted retinal drug delivery based on diffusion from a surface-coated microrobot docked to a blood vessel with a microneedle (18). Ergeneman et al. make the argument that functional surface coatings such as the oxygen-sensor and drug-delivery techniques described above, as opposed to MEMS devices, are desirable for intraocular microrobots (56). Holligan et al. propose controlling a group of magnetic particles collectively to act as a tamponading agent in retinal therapy (57). However, such magnetic particles must be proven nontoxic to the highly sensitive retina.

2.2.5. The ear. Microrobots have potential in the inner ear, which consists of the cochlea and the semicircular canals. The smallest dimensions of both the scala tympani and the scala vestibuli of the cochlea vary approximately linearly from ~1 mm at the beginning of the scalae to ~0.3 mm at a depth of 37 mm (58). The smallest cross-section of the horizontal semicircular canal can be approximated as an ellipse, whose major and minor axes are 0.37 and 0.27 mm, respectively (59).

Cochlear implants can restore hearing through the placement of electrodes into the scala tympani to stimulate the cochlear nerve. However, there is still significant room for improvement in sound quality with cochlear implants, and the current surgical procedures can cause a number of complications including trauma, infection, and even partial paralysis (60). It may be possible to improve cochlear implant procedures with wireless microrobotic techniques.

There is also a great deal of stem-cell research aimed at the generation of the cochlear hair cells that are responsible for natural hearing. However, the vast majority of this research is performed in vitro, and how to grow new hair cells in vivo is still unclear (61). A microrobot may be the appropriate vehicle to deliver the differentiated stem cells to their desired location.

2.2.6. The fetus. In a growing number of cases, open surgery on a growing fetus can prevent death or life-long impairments and malformations (62). Minimally invasive laparoscopic and robot-assisted surgery is difficult in the case of fetal surgery because of the extra surface through which the tool must pass (i.e., the wall of the uterus, in addition to the mother's abdomen), which limits the tool's DOF. In addition, there is an increased risk of preterm labor when the tool is larger than 2–3 mm (63). Microrobots may hold the key to the future of fetal surgery. Researchers have proposed a number of procedures that could be performed by a microrobot that enters the uterus through the cervix (62, 63). A microrobot could act as a temporary tracheal occlusion when the

growth of the fetus's lungs is pathological, it could perform ablation in cases of congenital cystic adenomatoid malformation to prevent hydrops, and it could act in cases in which the urinary tract of the fetus has an obstruction that must be cleared. A microrobot might even replace the needles used in amniocentesis and cordocentesis.

MTB: magnetotactic bacteria

3. POWERING MICROROBOTS

For a technical discussion on the design of wireless microrobots, we must begin with power. With microrobots, even more so than with traditional robots, we must be acutely aware of the methods available to store, harvest, and transmit power, and we must acknowledge the strict limitations that power consideration will put on any practical design. Without addressing power from the beginning, it is difficult to transition from prototypes to fully miniaturized wireless devices.

3.1. Onboard and Scavenged Power

Batteries offer an inexpensive power source, but because the total deliverable energy scales with volume, they are not promising. Rechargeable thin-film batteries are a type of battery possibly suitable for microrobotic applications. Thin-film batteries differ from traditional batteries in that they are fabricated through the use of semiconductor technologies. These planar fabrication processes enable arbitrarily shaped batteries with thicknesses less than 50 μm. This allows design for optimal use of space.

MEMS-based power generators are of interest because they provide higher energy densities than traditional generators and batteries (64). Several research groups have presented transducers to convert various types of energy into electrical energy. Many make use of onboard chemical fuels, and others harvest mechanical energy from the environment in the form of vibrations. The Seebeck effect, in which a temperature gradient develops a voltage differential, makes thermal harvesting another potential option (65, 66). Developing a thermal gradient would require the microrobot to contain a hot source, which could be induced wirelessly through electromagnetic methods as discussed previously (see Section 2.1.1) or which could be generated by a hot radioactive source.

A desirable approach for powering medical microrobots would be to harvest chemical energy directly from the environment. Biofuel cells operate at low temperatures (~20–40°C) and in environments where the pH is almost neutral (67); these conditions resemble those of a healthy adult. Exploiting glucose and oxygen found in blood, an in vivo microrobot could be powered. (Extensive reviews of the state of the art in biofuel cells are available in References 67 and 68.) Muscle cells can also be used as simple actuators and have been utilized to actuate fabricated structures such as micropillars (69), cantilevers and legged microrobots (70), and other microdevices (71).

Instead of engineering the locomotion subsystem for the microrobot, researchers can directly utilize microorganisms that are able to swim. Martel and colleagues (72) recently demonstrated that a clinical MRI system can be used to localize and control a swarm of magnetotactic bacteria (MTB). The individual propulsive force generated from a single bacterium was found to exceed 4 pN, resulting in no-load swimming speeds exceeding 200 μm s^{-1}. Various strategies are proposed to functionalize the MTB, including attaching nanoparticles to the MTB, loading the inside of individual MTB, pushing or pulling an attached micro-object with one or more MTB, or using a swarm of MTB to move an unattached object. The method used to control the MTB (although not power them) is similar to that discussed in Section 4.4. Challenging issues such as control of the orientation of bacterial adhesion to a desired object and generation of sufficient forces must still be addressed.

3.2. Transmitted Power

An alternative approach is to design little or no power storage or generation into the microrobot, and to instead wirelessly transmit power to the device. This is most easily done through the use of magnetic fields. In one method, time-varying magnetic fields are used to induce currents, creating a wireless method for electricity generation. In another, quasi-static and low-frequency magnetic fields are used to apply forces and torques directly to magnetic materials. The human body is "transparent" to magnetic fields (73, 74), which means that the magnetic permeability of the human body is approximately the same as that of air vacuum, so there are no significant interactions of tissue with low-frequency magnetic fields as opposed to electric fields.

3.2.1. Induction. The basic principle of transmitting electrical power with magnetic fields is based on Faraday's law of induction. When current is flowing in a circuit (primary), a magnetic field is generated in its surroundings. An effective voltage source develops in any nearby circuit (secondary) given by

$$V_2 = -\frac{d\Phi_{21}}{dt}, \quad \Phi_{21} = \int_{S_2} \vec{B}_{21} \cdot d\vec{S}_2, \tag{1}$$

where $\vec{B}_{21}$ is the magnetic flux density at the secondary generated by the primary, and Φ_{21} is its flux through the secondary (75). The flux density is linearly related to current in the primary. The developed voltage results only from the time-varying component of the primary current, which in practice is sinusoidal, and the geometry that determines the flux Φ_{21} crossing the secondary surface S_2. Equation 1 simplifies to $V_2 = M \cdot di_1/dt$, where i_1 is the current of the primary inductor and M is the mutual inductance between the two coils, entirely dependent on geometry (distance between the coils, angular and radial misalignment, and so on). For maximum power transfer between the two circuits, they must be tuned to resonate at the same operating frequency (76).

One can increase the induced voltage by increasing the frequency of the primary current or its amplitude, or by modifying the geometry of the circuit arrangement. Increasing the primary current amplitude generates a stronger field, but there is an upper limit on the field strength dictated by safety regulations (27, 77). Increasing the area of the secondary circuit or by bringing it closer to the primary results in an increased flux (M increases).

Many mesoscale devices already incorporate this principle (76, 78, 79). Large coils outside the body generate a varying field that is captured by small coils embedded in capsules. However, at the microscale, the challenge is in the design of the receiver coils because they are constrained by planar microfabrication processes. Additionally, the efficiency of voltage rectification on the receiver side becomes increasingly important as the device scales down because the developed voltage amplitude decreases as well.

3.2.2. Magnetic force and torque. Rather than generate electricity with magnetic fields, we can apply forces and torques directly to magnetic materials. The force $\vec{F}$ in Newtons (N) and torque $\vec{T}$ in Newton meters (N m) developed on a magnetic material are given by

$$\vec{F} = \int_V (\vec{M} \cdot \nabla)\vec{B} dV \approx (\vec{D} \cdot \nabla)\vec{B} \tag{2}$$

and

$$\vec{T} = \int_V \vec{r} \times (\vec{M} \cdot \nabla \vec{B}) dV + \int_V \vec{M} \times \vec{B} dV \approx \vec{D} \times \vec{B}, \tag{3}$$

where $\vec{B}$ is the flux density of the applied magnetic field in Tesla (T), $\vec{M}$ is the magnetization of the material in Amps per meter (A m^{-1}), and the integration is carried out over the material's

volume V in cubic meters (m^3) (80). It is also possible to describe the applied magnetic field $\vec{H}$ in Amps per meter ($A\ m^{-1}$), where $\vec{B} = \mu_0 \vec{H}$ and $\mu_0 = 4\pi \times 10^{-7}\ T\ m\ A^{-1}$ is the permeability of free space. When the geometry of the magnetic material is small relative to the spatial changes in the applied magnetic field—which is realistic for wireless medical microrobots being powered by externally generated magnetic fields—the magnetic field can be modeled as uniform across the small microrobot. In addition, the magnetization of the material, which generally varies across the body, can be modeled as constant throughout the body with a value equal to the average magnetization. It is also often convenient to think of the total dipole moment $\vec{D}$ of a magnetic body, which is simply the product of the volume of material and the average magnetization, leading to the approximations in Equations 2 and 3. The strength of the magnetic force and torque is directly proportional to the strength of the applied field, the magnetization of the material, and the volume of material.

Ferromagnetic materials can generally be classified as either soft or hard. All have a value of magnetic saturation, which is the maximum possible magnetization of the material. All exhibit hysteretic behavior. The magnetization of soft-magnetic materials is highly dependent on the instantaneous applied field, and they tend to return to their nonmagnetized state when the applied field is removed. Ideal soft-magnetic materials have negligible hysteresis. Significant hysteresis is exhibited by hard-magnetic materials, which retain much of their magnetization once magnetized, independent of the current applied field. The magnetization remaining when the applied field is removed is known as the remanence M_r. The applied field required to demagnetize the material is known as the coercivity H_c. Ideal hard-magnetic materials, which are used for permanent magnets, have a high coercivity, and high remanence makes for strong permanent magnets.

Every magnetic body has geometric effects that make its magnetic properties differ along different directions within the body. This is known as shape anisotropy. Demagnetizing fields tend to weaken magnetization, and demagnetizing fields are largest along short directions of the body. A long direction in a body is thus termed an easy axis because it is a relatively easy direction in which to magnetize the material. In soft-magnetic bodies, magnetic torque tends to align an easy axis with the applied field. Other types of anisotropy exist, such as crystalline anisotropy, but these are typically dominated by shape effects, even at the scale of medical microrobots.

Understanding the fields required for wireless control of permanent magnets is relatively straightforward because the magnetization of the material can be accurately modeled as constant and rigidly attached to the body. The magnetization of soft-magnetic bodies is more complicated. However, accurate analytical models of magnetic force and torque, appropriate for real-time control of microrobots, now exist for soft-magnetic, axially symmetric bodies (e.g., beads, ellipsoids, cylinders) (81) and for soft-magnetic bodies assembled from thin planar components (82). Soft-magnetic materials are easier to microfabricate than permanent magnets, making them desirable in microrobot design. However, in cases where the applied field is too weak to saturate the soft-magnetic material, microrobots that incorporate permanent magnets may prove more effective.

The magnetic field generated by a magnetic dipole is dependent on the geometry of the body. However, an analytical model named the point-dipole model serves to model the field of a magnetic body:

$$\vec{H}(\vec{P}) = \frac{1}{4\pi |\vec{P}|^3} \left(\frac{3(\vec{D} \cdot \vec{P})\vec{P}}{|\vec{P}|^2} - \vec{D} \right). \quad (4)$$

$\vec{P}$ is the vector from the point dipole to the position of interest in meters (m), and $\vec{D}$ is the magnetic dipole moment in Amp meters squared ($A\ m^2$). The magnetic field of a sphere can be perfectly modeled with a point-dipole model, and the fields of other geometries approach that of a point

dipole at increasing distance from the magnetic body. The strength of the magnetic field decreases as $\sim |\vec{P}|^{-3}$, which imposes a significant limitation in projecting strong magnetic fields.

RF: radio frequency

A current-carrying loop is also a magnetic dipole. The dipole moment of a closed current-carrying loop is equal to the product of the current and the area of the loop. For a circular loop of radius r and current i, the dipole moment is simply $|\vec{D}| = \pi i r^2$, with the direction of $\vec{D}$ pointed along the axis of the loop and defined by the direction of current flow using the right-hand rule (80). The dipole moment $\vec{D}$ will attempt to align with an external magnetic field as in Equation 3.

3.2.3. Safety of magnetic fields. The greatest threat posed by high-static fields is nearby ferromagnetic objects acting as projectiles (27). The nonexperimental recommended maximum field strength for MRI procedures is 4 T under medical supervision. Time-varying fields are associated with induced electric fields related to $d|\vec{B}|/dt$, the rate of change of the field strength, and the highest risk is cardiac fibrillation resulting from nerve stimulation. The recommended maximum rate change (in Tesla per second) for controlled operation is given by

$$\frac{d|\vec{B}|}{dt} = 20\left(1 + \frac{0.36}{\tau}\right), \tag{5}$$

where τ is the period (in milliseconds) of the monotonically increasing or decreasing gradient (27). For normal operation, the above value should be reduced by 20%. Typical spatial gradient maximum values for whole-body MRI equipment currently reach 10–50 mT m^{-1} with a switching time of 0.1–1 ms. Radio frequency (RF) coils are related to heat absorption, and the main concern is increase in body temperature. The recommendations are given in terms of the specific absorption rate (SAR). For normal operation and an averaging period of 6 min, the maximum recommended whole-body SAR is 2 W kg^{-1}, whereas for the head (averaged over any 10 g of matter) the local recommended SAR is 10 W kg^{-1}. In any case, the 10-s short-term SAR level should not exceed 3 times the corresponding recommendation (27).

4. MICROROBOT LOCOMOTION

For microrobots to locomote within the body, power must be transduced into motion. Locomotion methods of medical microrobots must be designed with their working environment in mind; that is, they must be designed to work in fluid-filled lumens and cavities and in soft tissues. Microrobot locomotion must also utilize methods that are scale appropriate.

It is well known that swimming at the microscale requires techniques that differ greatly from those used by macroscale swimmers such as fish and humans (9). To understand this phenomenon, we turn to the Navier-Stokes equations, which, when combined with boundary conditions, completely define a fluid's flow. For a fluid with constant density ρ and constant viscosity η, the Navier-Stokes equations are given by a single vector equation, which can be nondimensionalized in space and time by the magnitude of the free-stream velocity $\mathcal{V}$ and some characteristic length $\mathcal{L}$:

$$\left(\frac{\rho \mathcal{V} \mathcal{L}}{\eta}\right)\frac{d\vec{V}}{dt} = -\nabla p + \nabla^2 \vec{V} \Rightarrow Re = \frac{\rho \mathcal{V} \mathcal{L}}{\eta}. \tag{6}$$

$\vec{V}$ is the velocity vector field and p is the hydrodynamic pressure scalar field, which have both been nondimensionalized as in Reference 83. From this equation, we discover the Reynolds number (Re), the dimensionless quantity that embodies the interaction between a fluid's inertia and its viscosity. At low Re, we are in a world that is either very viscous, very slow, or very small. A microrobot's world is dominated by low velocities and small scales. Low-Re flow around a body is termed creeping flow or Stokes flow. We no longer see a transition to turbulence, even behind

bluff bodies. At low *Re*, the role of time becomes negligible in Equation 6; the flow pattern does not change appreciably whether it is slow or fast, and the flow is nearly reversible. Consequently, reciprocal motion (i.e., body motion that simply goes back and forth between two configurations) results in negligible net movement (9).

In contrast to high-*Re* flows, in low-*Re* flows the presence of any wall becomes increasingly important. For flows where $Re < 1$, the wall effect on a moving body can only be neglected if $s \cdot Re > 20\mathcal{L}$, where $\mathcal{L}$ is the same characteristic length used in Equation 6 and s is the distance of the body from the closest wall (84). It is easy to see that at low *Re*, a wall that is many body lengths away can affect the swimming of a microrobot compared with how it would swim in open fluid. The assumption of open fluid is typically assumed in published analytical models of low-*Re* swimming, but there are some methods that compensate for the presence of walls.

We can turn to nature for inspiration for possible microrobot swimming methods. Microorganisms have evolved a variety of mechanisms to swim at low *Re*, none of which are found in macroscale swimmers (84). Bacteria use a molecular motor to turn the base of a flagellum that deforms into a helical shape. Eukaryotic cells have flagella that are active organelles with the ability to create rotating movements and traveling waves. Some microorganisms swim using cilia, which are active organelles that are held perpendicular to the flow during the power stroke and parallel to the flow during the recovery stroke, with many cilia being used simultaneously. All these swimming methods capitalize on the same phenomenon: Each element along the length of the flagellum slices through the fluid at an oblique angle, and it is the difference between parallel and perpendicular fluid drag with respect to this small cylindrical element, integrated along the length of the flagellum, that results in net propulsion. To date, no microrobot propulsion scheme has mimicked the behavior of cilia. However, schemes have emulated the behavior of bacterial and eukaryotic flagella; these are discussed in detail below.

4.1. Helical Propulsion

Inspired by bacterial flagella, a number of microswimmer designs use some form of helical propeller for locomotion. The method that most closely resembles a bacteria in function uses a rotary motor to turn a passive flagellum (**Figure 4*a***). However, miniaturizing such a motor-driven system is difficult. The generation of torque using external magnetic fields has proven to be a successful method for helical propulsion in a number of studies, including at the microscale. **Figure 4*b*** demonstrates how a rotating magnetic field can be used to control a magnetic helical propeller. This method has been experimentally demonstrated using permanent-magnetic (85, 86) and soft-magnetic materials (87, 88) in a wide range of sizes.

Regardless of the method used to apply torque, there are options in the fabrication of the helical propeller. The propeller can be made rigid—possibilities range from a simple wire formed into a helix (85) to a multilayer strip that self-forms into a helix because of internal stresses (87, 88). The efficacy of the propellers is insensitive to the helix cross-section (9). With rigid propellers, the direction of microrobot motion can be reversed simply by reversing the rotation direction. That is, rigid propellers are capable of both pushing and pulling a body.

The propeller may also be compliant and have a helical geometry only dynamically. A simple fiber, after crossing some threshold of torsion, will experience a bifurcation that results in the fiber twisting up into a helical geometry, which is maintained until the torsion is removed. This method will result in swimming that is less controllable than swimming with a rigid helical propeller. With the exception of some short-term tumbling motions similar to actual bacterial swimming, the compliant helical propeller can only push the body, and consequently, reversing course is more difficult than doing so with a rigid propeller. However, this type of compliant propeller opens up

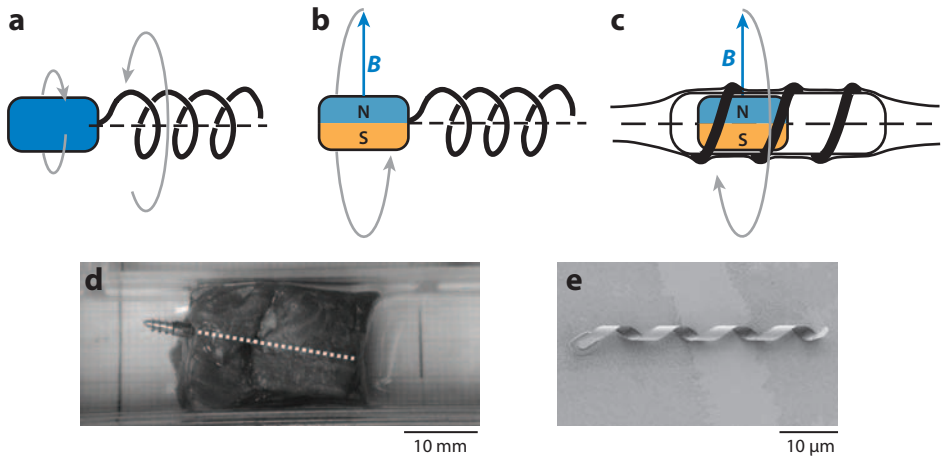

Figure 4

Helical propulsion. (*a*) A rotary actuator turns the propeller with respect to the microrobot body. As the propeller rotates, the body counterrotates. (*b*) The propeller is rigidly attached to the microrobot body, which is rotated by a magnetic field *B*. N and S indicate the north and south poles of the magnetic body. (*c*) Helical propulsion to crawl through lumens or tissue, based on Reference 89. Magnetic fields are used to rotate the rigid microrobot body. (*d*) The magnetic screw-type microrobot of Reference 90 running through bovine meat. Image courtesy of Kazushi Ishiyama, Tohoku University. (*e*) The soft-magnetic helical microswimmer of Reference 88.

additional possibilities in microrobot design, such as the use of long strips of drug that will twist up into a helical shape, allowing the payload of the microrobot itself to act as the helical propeller (91).

Helical propulsion also provides an effective method to move through lumens through a strategy that is closer to crawling than swimming (89). As shown in **Figure 4*c***, by pressing against the walls of a deformable lumen, the microrobot moves much like a bolt moves through a threaded nut. If the lumen wall is slippery, the helix will slip obliquely, but the microrobot will still advance, although more slowly, in a manner analogous to helical-propeller swimming (92).

There is another magnetically driven helical-propulsion strategy that is similar but distinct from the helical-propeller swimming mechanism described above. A screw-shaped microrobot—modeled on either a wood screw or a corkscrew, with embedded magnetic material—can be driven wirelessly through tissue as shown in **Figure 4*d***. These screw-shaped microrobots represent a viable option for moving through soft tissues. Whereas the helical propeller of a swimming microrobot slices through fluid obliquely, the helix of a screw-type robot moves through tissue as a wood screw or a corkscrew would. Consequently, a screw-type microrobot that performs one complete revolution as it moves through tissue advances by exactly one pitch of the helix, whereas a helical swimmer must perform multiple revolutions to advance by one pitch length. It has also been demonstrated that screw-shaped microrobots can swim through fluid. The swimming principle is comparable with that of the helical-propeller swimmers described above.

For any of the above implementations of rigid helical propellers, some common behaviors emerge. Let us consider swimming along the axis of the helix. At low *Re*, the external nonfluidic force f and nonfluidic torque τ that act on a helical swimmer are linearly related to its linear and rotational velocities v and ω by a symmetric matrix (9):

$$\begin{bmatrix} v \\ \omega \end{bmatrix} = \begin{bmatrix} a & b \\ b & c \end{bmatrix} \begin{bmatrix} f \\ \tau \end{bmatrix}. \quad (7)$$

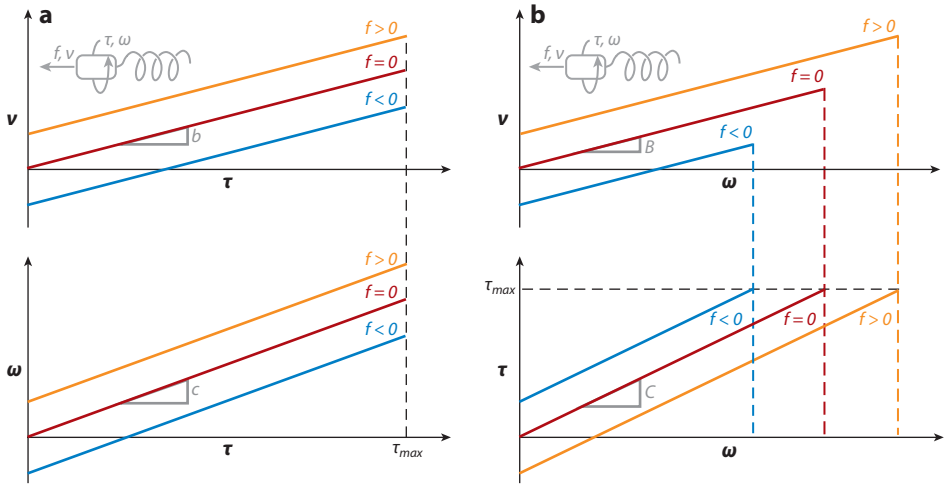

Figure 5

(*a*) Qualitative behavior of helical-propeller swimming, with applied torque as the control variable. Parameters are defined in Equation 7. This representation is particularly useful when considering helical propellers driven by rotational rotary actuators (e.g., motors). (*b*) Qualitative behavior of helical-propeller swimming, with rotational frequency as the control variable. Parameters are defined in Equation 8. Sign convention is defined in the inset image of the swimmer, whose two arrows show which way positive movements are defined. This representation is particularly useful when considering helical propellers driven by applied magnetic fields.

The matrix coefficients have been explicitly calculated for cases in which the flagellum is rigidly attached to the body (93) and in which the body counterrotates with respect to the flagellum (94). In the case of a motor-driven flagellum, the fundamental control input is the torque τ, and the nonfluidic applied force f can be thought of as the second input. **Figure 5*a*** shows how swimming velocity, both forward and rotational, are affected by τ and f, and how the maximum torque generation limits the overall swimming performance.

In the case of magnetically applied torques, the rotation frequency of the magnetic field is the fundamental control input. The microrobot rotates in sync with the applied field, nearly instantaneously reaching an equilibrium phase shift such that the magnetic torque perfectly counterbalances the fluidic drag torque. It is more instructive in this case to rearrange the linear equations with the nonfluidic applied force f and rotational velocity ω as the input variables:

$$\begin{bmatrix} v \\ \tau \end{bmatrix} = \begin{bmatrix} A & B \\ -B & C \end{bmatrix} \begin{bmatrix} f \\ \omega \end{bmatrix}. \tag{8}$$

Equations 7 and 8 are related by $A = a - b^2/c$, $B = b/c$, and $C = 1/c$. **Figure 5*b*** shows the behavior observed with this type of swimming. The forward velocity grows linearly with frequency until a "step-out" frequency is reached. Beyond this step-out frequency, the available magnetic torque is no longer sufficient to keep the microrobot rotating in sync with the applied field, and a drastic decrease of the swimming velocity is observed. This behavior has been demonstrated experimentally at a number of scales.

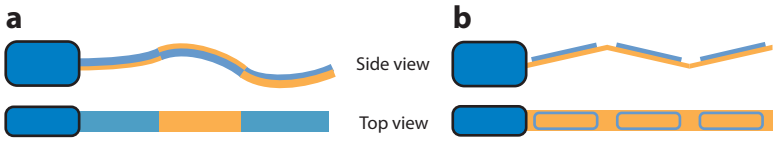

Figure 6

Traveling-wave propulsion with distributed actuation. (*a*) Piezoelectric bilayer actuators create local bending (43). (*b*) Current-carrying coils create local torques that attempt to align the coils with an applied magnetic field (95).

4.2. Traveling-Wave Propulsion

Inspired by eukaryotic flagella, a number of microswimmer designs attempt to create a traveling wave to generate propulsion. Traveling waves provide an effective means of propulsion at low *Re* and are even more efficient than helical propellers, assuming equal actuation efficiency (94). However, implementing a true traveling-wave propeller at the microscale is difficult. Creating the type of distributed actuation seen in eukaryotic flagella is difficult in terms of fabrication, power, and control. Some methods create traveling waves without distributed actuation, making microfabrication and wireless control more feasible, but the swimming efficiency is reduced.

One method to construct a traveling-wave propeller involves distributed piezoelectric actuators (43). Each individual actuator comprises a bilayer. When one layer is put in tension and the other is put in compression, the result is local bending of the actuator (**Figure 6*a***). As the number of piezoelectric actuators is increased, the behavior of the propeller approaches continuous actuation, and the ability to implement more complicated waveforms increases, but only two actuators are required to implement a simple traveling wave. One can control the direction of motion by controlling the actuation sequence of the actuators; thus the propeller can both push and pull an attached body, and reversing the swimming direction is simple. However, this type of design presents challenges in downscaling, both in terms of power generation and wireless control.

Another proposed method of distributed actuation takes a hybrid approach that makes use of both electrical power and a strong, static applied magnetic field (95). The method works by distributing electrically conducting coils along the length of the propeller (**Figure 6*b***). The flow of current through an individual coil induces a magnetic moment that attempts to align the coil axis with the applied magnetic field. When the current flowing through the coils is controlled independently, a traveling wave is created. Again, the propeller can both push and pull an attached microrobot body. One desirable property of this type of propulsion for wireless locomotion is that an increase in the strength of the applied magnetic field allows an equal decrease in the required electrical current flowing through the coils to generate the same local magnetic moments. Thus, increasing the strength of the static magnetic field would allow a greater portion of the propulsive power to be transmitted wirelessly. This propulsion scheme has the potential to be powered by a clinical MRI system, which is discussed further in Section 4.4.

As previously mentioned, creating traveling-wave propellers with distributed actuation is difficult at the microscale, especially considering power. However, there are methods that can mimic some of the desirable properties of eukaryotic flagella with the use of only a single actuator. The use of an elastic tail (also termed a flexible oar) requires only a single actuator at one end, but the efficiency of a traveling wave created with an elastic tail will fall short of that created with distributed actuation. In general, a propeller that is too short and rigid will result in reduced net propulsion because the oscillating movement is essentially reciprocal. If the propeller is too long and flexible, there is reduced net movement because of an increase in drag relative to propulsion.

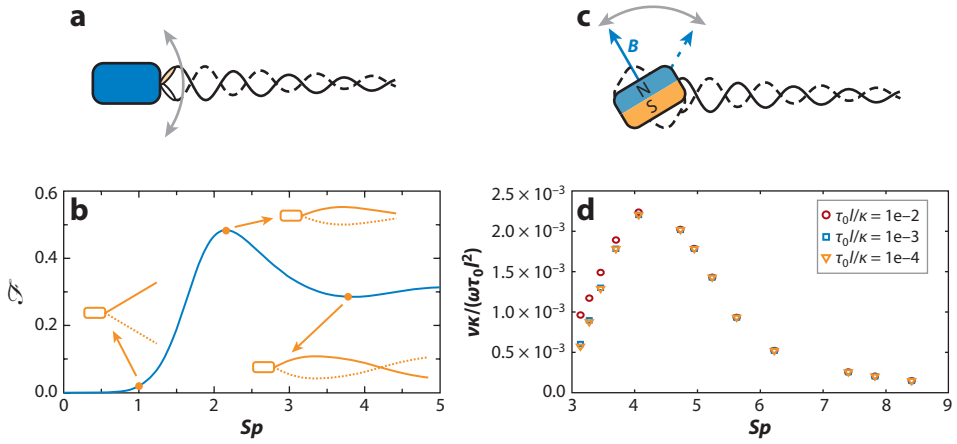

Figure 7

Traveling-wave propulsion with an elastic tail. (*a*) An internal actuator oscillates the tail with respect to the microrobot's body. (*b*) Nondimensional propulsive force $\mathcal{F}$ versus Sp for stationary, sinusoidally driven elastic tails. Image courtesy of Tony S. Yu, Massachusetts Institute of Technology, based on Reference 96. (*c*) Utilization of oscillating magnetic fields to actuate the tail. B represents the applied field. (*d*) Numerical simulations of an elastic tail being driven by a pure sinusoidal torque at one end, showing dimensionless velocity normalized by dimensionless torque versus Sp (93).

For elastic-tail swimmers, the actuator induces a wave that then travels away from the actuator, such that the propeller always pushes on the attached body.

In one conception of elastic-tail propulsion, an onboard actuator oscillates the proximal end of the propeller with respect to the microrobot's body, as shown in **Figure 7*a***. This type of actuation has been analytically considered in detail but has not yet been implemented in a microscale prototype. Yu et al. explore the propulsive force of an elastic tail being driven with a sinusoidal angle of $\phi = \phi_0 \sin(\omega t)$ with the position of the proximal end fixed (96). They find that elastic tails have an optimal length/stiffness/frequency combination, termed an optimal floppiness, which is quantified by the dimensionless Sperm number $Sp = l\,(|\omega|\xi_\perp/\kappa)^{1/4}$, where l is the length of the tail, κ is the bending stiffness, and $\xi_\perp$ is the drag coefficient for flow perpendicular to the tail. They report an optimal value of $Sp = 2.1$, and they also find excellent agreement between theoretical, numerical, and experimental results. The dimensionless force $\mathcal{F}$ is shown as a function of Sp in **Figure 7*b***, where the dimensionless force is given by

$$\mathcal{F} = f\left[\frac{1}{\phi_0^2\left(\xi_\perp - \xi_\parallel\right)}\left(\frac{\xi_\perp}{\kappa|\omega|}\right)^{1/2}\right], \tag{9}$$

where f is the propulsive force and $\xi_\parallel$ is the drag coefficient for flow parallel to the tail. The insets show the qualitative shape of the optimal and suboptimal waveforms; note the suboptimality of the waveforms depicted in **Figure 7*a***. Lauga numerically considers the case of free swimming (97). He reports optimal Sperm numbers in the range $Sp = 2.5$–3.3, depending on the shape of the microrobot body and the choice of the optimality metric. He also reports on the optimal tail length for a given body size; for a spherical body of radius r, the optimal length is in the range $2.7r$–$5.6r$. In the case of free swimming, the body counterrotates, analogous to the mechanism shown in **Figure 4*a***.

It is also possible to power and control an elastic tail wirelessly with magnetic fields. A field can be used to generate a torque on magnetic material that is rigidly embedded in the microrobot's

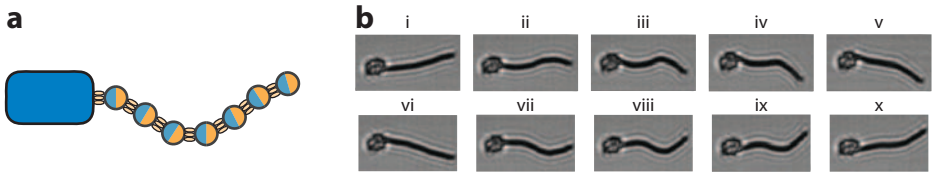

Figure 8

The microscopic artificial swimmer of Reference 100. (*a*) A chain of paramagnetic beads attached to one another by DNA can be used as a traveling-wave propeller to pull an attached body. The shape of the chain is influenced by an applied magnetic field. (*b*) Experimental motion sequence of such a propeller pulling a red blood cell. Image courtesy of Rémi Dreyfus, New York University.

body (98, 99). A time-varying oscillating field causes the body to fluctuate, which induces a wave motion in the tail as depicted in **Figure 7*c***. The mean orientation of the oscillating field dictates the swimming direction of the microrobot. **Figure 7*d*** shows that numerical results for this type of swimming predict optimal swimming at similar *Sp* values (93). Rather than rigidly connect the magnetic material to the microrobot's body, one can instead construct an onboard actuator, based on the scheme shown in **Figure 7*a***, using this type of magnetic method.

A final type of traveling-wave propulsion, which has already been demonstrated at the microscale, combines elements from distributed actuation and elastic tails. A chain of paramagnetic beads attached to one another by DNA form an artificial flagellum that is responsive to applied magnetic fields (100). This propeller can be attached to a desired payload, which in the original work was a red blood cell but can also be a microrobot body (**Figure 8**). The beads tend to align to an externally applied magnetic field, and oscillating the field induces a wave motion in the chain of beads. The direction of movement is such that the propeller always pulls the attached body, as the wave travels from the distal end of the propeller toward the body. Other researchers have provided additional analysis of this swimming method (101–103). It is the relatively large drag of the attached payload that creates the nonreversing propeller movement responsible for the net movement of the body. Without an attached body, the propeller has negligible net movement. However, it has been shown that a defect in one of the elastic connections between the beads can lead to net movement of the propeller, even without an attached body.

4.3. Pulling with Magnetic Field Gradients

We have shown how magnetic fields can be used to help mimic swimming methods of microorganisms without the need for any onboard actuation. Magnetic fields also provide us with an actuation method that is impossible for autonomous microorganisms and that consequently has no direct analogy in nature: wireless pulling through the use of field gradients. Magnetic fields have been used to apply forces and torques on magnetic objects in medical applications for quite some time (104).

Controlled magnetic fields can be generated in a variety of ways. The first method uses electromagnets that are simultaneously position and current controlled. In a study by Grady et al. (39), a permanent-magnet seed was controlled in vivo in a canine brain through a single position-controlled electromagnetic coil. In Yesin et al. (55), the uniform field of a pair of electromagnetic coils is superimposed with the gradient field developed by a second pair of coils. The two coil pairs, which are rigidly connected, are position controlled to manipulate a magnetic microrobot. A second method uses stationary current-controlled electromagnets. In Meeker et al. (41), three orthogonal pairs of coils are used in a "helmet" configuration to control magnetic fields throughout

a human head, as a stated improvement to the design in Grady et al. (39). However, this helmet design allows only partial control because full torque and force control is not possible owing to singularities in the workspace. It has also been shown that the electromagnetic coils in a clinical MRI system can be used to position ferromagnetic beads (32), and in vivo animal experiments have already been performed (33). A third method uses position-controlled permanent magnets. This is the method used by the Stereotaxis Niobe Magnetic Navigation System, which is used to steer magnetic-tip catheters (105).

Analytical models for the magnetic force and torque on soft-magnetic axially symmetric bodies and assembled-MEMS bodies are provided in References 81 and 82, respectively. An advantage of soft-magnetic assembled-MEMS microrobots, which consist of a set of electroplated planar components that are assembled after microfabrication, over simpler soft-magnetic beads is their ability to easily become magnetized because of strong shape anisotropy. An assembled-MEMS microrobot of the type built in studies by Yesin et al. and Nagy et al. (55, 82) will reach magnetic saturation in an applied field that is only a small fraction of the strength of the field needed to saturate a spherical bead made of the same material. This makes wireless control of assembled-MEMS devices more feasible than that of beads over long distances. An additional benefit of assembled-MEMS microrobots over beads is the ability to incorporate additional MEMS functionality into the components. However, the relatively small quantity of soft-magnetic material contained in an assembled-MEMS microrobot, compared with a solid geometry with the same overall footprint, makes applying magnetic force relatively more difficult.

A group of nanoparticles can also be controlled much as a single microrobot can be controlled. This group may provide increased ability to deform in order to avoid obstacles and move through a small opening—and even to penetrate into and move through tissue (106, 107).

Because pulling with magnetic field gradients has no analogy in microorganisms, it is reasonable to conjecture that it might provide a more effective means of wireless propulsion than anything that could evolve through natural selection. However, it has been theoretically shown (93) that microrobots that swim with magnetically driven helical propulsion or magnetically driven elastic-tail propulsion are more promising for medical applications compared with pulling on the microrobot directly with magnetic field gradients as the microrobot's size is decreased for two key reasons. First, although maximum speed and force generation both decrease as the size of the microrobot is reduced, the decreases are more rapid with field-gradient pulling. Second, it is easier to project magnetic fields over large distances than it is to project field gradients; recall from Equation 4 that the field decays with distance from its source as $\sim|\vec{P}|^{-3}$, and a spatial derivative of the field results in a field gradient that decays as $\sim|\vec{P}|^{-4}$.

4.4. The Clinical Magnetic Resonance Imaging System

As we consider magnetic control of medical microrobots, it is natural to turn our attention to clinical MRI systems. These powerful magnetic systems already exist in many clinical settings, and utilizing them for microrobot control with few modifications would eliminate the need for custom hardware and increase the likelihood of clinical acceptance of the new microrobotic technology. In addition, being primarily an imaging tool, the MRI system already provides a potential method for localization.

A clinical MRI system has the ability to generate large magnetic fields, but its construction puts limits on the types of microrobot control that are possible. Let us briefly consider the construction (108). The system creates a strong uniform field aligned with its bore that is constant during operation, with typical field strengths of 1.5 T or stronger. We refer to the bore direction as the z direction (**Figure 9**). Because the field is aligned with the bore, the magnitude of the magnetic field

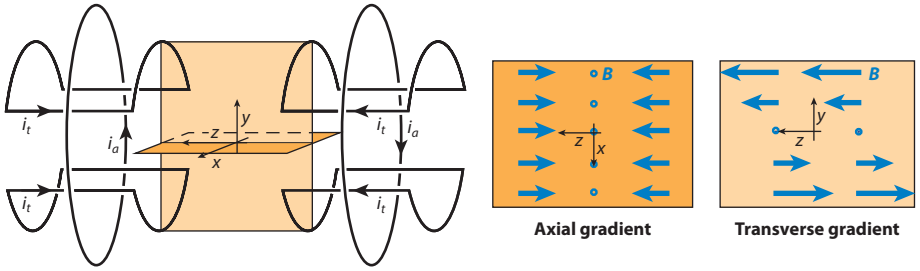

Figure 9

Schematic of the clinical magnetic resonance imaging system and its typical configuration of gradient coils. Uniform axial gradients are generated by a pair of Maxwell coils operating with current i_a. Uniform transverse gradients on the z-y plane are generated by double-saddle coils, commonly known as Golay coils, operating with current i_t. Another pair of Golay coils rotated by 90° about the z axis (not shown) generates transverse gradients in the z-x plane.

is equal to the component of the field along the z axis: $B_z = |\vec{B}|$. The MRI system also contains three sets of coils for the generation of gradients in the field; the fields of these coils superimpose with the strong uniform field. The field contributions of the gradient coils do not change the direction of the magnetic field; instead, they change the magnitude of the field throughout the workspace. This allows us to think of the gradients as simple scalar derivatives: $\partial B_z/\partial x$, $\partial B_z/\partial y$, and $\partial B_z/\partial z$. These three gradients can be changed independently and relatively quickly. Finally, RF coils are utilized to drive proton spin to resonance to read out the received signal during relaxation. The design requirements for RF coils vary with the objective of the MRI screening. Surface RF coils are widely used mainly as receiver coils because of their high sensitivity, but the penetration depth they can reach is low.

One potential use of an MRI system for microrobot control utilizes the strong bore field combined with the gradient coils to implement the gradient-pulling method described in Section 4.3. Wireless propulsion of soft-magnetic beads has been demonstrated (32), and experiments in a living swine have already been conducted (33). Regardless of whether the microrobot contains a permanent magnet or soft-magnetic material, the strong field along the bore will align the microrobot's magnetization with the z axis. Because we cannot control the direction of the field—we can control only the magnitude—the MRI system limits us to applications in which we can accept this constant alignment. This limits applications to three cases: a permanent magnet whose dipole is always aligned with the bore, a soft-magnetic body whose long (easy) dimension is always aligned with the bore, or soft-magnetic spheres. If any of these three cases is acceptable, the applied force can be controlled directly using the three current-controlled field gradients

$$\vec{F} = |\vec{D}| \cdot \left(\frac{\partial B_z}{\partial x}, \frac{\partial B_z}{\partial y}, \frac{\partial B_z}{\partial z} \right), \tag{10}$$

where the dipole strength $|\vec{D}|$ of the microrobot can be considered constant.

Even with the large fields inside an MRI system, overcoming fluid drag in the bloodstream proved difficult. This difficulty arises from the fact that the gradient coils, which are fundamental to gradient-pulling methods, are not nearly as strong as the primary bore field. It has been suggested that the microrobot shape could be optimized to reduce fluid drag relative to magnetic forces, but a simple sphere has only ∼10% higher fluid drag than the optimal shape, so focusing on this aspect of the design is not likely to yield significant improvements (109).

Another potential use of an MRI system for microrobot control utilizes the strong bore field combined with the RF coils. In Section 4.2 we introduced a traveling-wave propulsion method

that uses coils distributed along the length of a propeller, each of which attempt to align with an applied magnetic field when carrying current. Kósa et al. (95) proposed that the RF coils of an MRI system could be used to wirelessly power the electronics onboard the microrobot, which in turn would supply the current to the individual coils. The coils would then attempt to align with the strong MRI bore field, and a wave motion would be induced through control. This scheme is still in the conceptual phase.

5. LOCALIZING MICROROBOTS

Various localization methods have been proposed to localize and track a microrobot inside the human body. Spatial resolution is an important factor in the determination of the microrobot's position. This resolution is indicative of position and/or orientation error, so the resolution is preferably in the submillimeter range for our microrobots, which span a few millimeters at most. Noise- and artifact-robust methods are preferred. The maximum rate at which the position estimation can be updated is also an important factor for real-time control.

5.1. Vision

The only location where the circulatory system is observable from the outside of the body is the retina of the eye. This makes imaging and localizing intraocular microrobots possible through simple components such as microscopes and cameras combined with image-processing techniques. However, the complicated optics of the human eye make accurate localization difficult. One proposed method for tracking an intraocular microrobot uses a purposely defocused view acquired from a single microscope (110). However, this method does not properly account for the optics of the eye. A custom single-aspheric-lens ophthalmoscope has proven better for the generation of wide-field-of-view focused images and for localization (111). Detecting and segmenting a metallic microrobot from the retinal background can be accomplished using color-space techniques (112).

5.2. Electromagnetic and Magnetic

The underlying principle in electromagnetic tracking is the use of a pair of devices: One acts as a field generator, and the other acts as a sensor (113, 114). The generator emits a low-frequency electromagnetic field that induces a voltage on the pick-up coils of the sensor. Because this voltage is a function of distance and orientation, localization is possible.

The accuracy of these systems depends on the presence of other objects. Material properties, shape, size, and position of these objects relative to the field generator or sensor are important factors that need to be considered (115). The frequency used for localization is also important because it has been shown that nearby materials affect accuracy in a unique manner (116).

It is often the case that the sensor is embedded in the device to be tracked, thus increasing the complexity of the design. Therefore, for wireless medical microrobots, magnetic tracking is an alternative methodology. A magnet is encapsulated in the device to be tracked, and an array of external magnetoresistive sensors are used to measure the magnet's field (117). The implicit assumption is that the magnet behaves as a magnetic point dipole, so its field in space is given by Equation 4. The assumption is valid when the measurement is performed at a large distance compared with the body length of the magnet. In the case of a magnetic sphere, Equation 4 is exact.

Magnetic tracking is a promising technique when there are line-of-sight problems, because the human body is transparent to static and low-frequency magnetic fields. However, solving the

inverse problem—i.e., finding the position by measuring the field—is not trivial (118) because of the nonlinear nature of Equation 4. To minimize the effect of background noise, calibration is usually required before the actual implementation of the tracking algorithm (117).

CT: computed tomography

PET: positron emission tomography

5.3. Magnetic Resonance Imaging

We have already shown in Section 4.4 how a clinical MRI system can be utilized to provide microrobots with locomotion capabilities. The same equipment can be used for localization. Groups of nanoparticles were localized in an MRI system in Kalambur et al. (107), and swarms of magnetotactic bacteria were localized as single objects in Martel et al. (72). The spatial resolution of the MRI system is similar to that of the early multislice computed tomography (CT)system (119), reaching 0.25 mm $\times$ 0.25 mm $\times$ 1.5 mm in a 3.0-T MRI machine (120). In the same work, an isotropic resolution of 0.57 mm was achieved, but the scan time was 25 s, which is probably too long for microrobotic applications. These values are in accordance with Azmi & Schulder (121), where the mean error of a 3.0-T MRI machine is less than 1.0 mm. The main drawback of MRI localization is that the choice of material for fabrication of the microrobot is limited (122). Ferromagnetic objects cause image artifacts that are sometimes larger than the object to be localized, even though information contained in spatial gradients can overcome this limitation (123).

5.4. Computed Tomography and Fluoroscopy

During a CT scan, the patient is placed between an X-ray source and a detector array, which records the attenuated X-ray beam as it passes through the patient's body (119, 124). A set of projected X-ray images gathered from various viewpoints is used to reconstruct the interior of the patient. CT scans offer very good low-contrast resolution and are capable of reconstructing the final image in 3D. Pixel resolution can reach 0.8 mm for a 512 $\times$ 512 pixel matrix (125), and more recently an isotropic pixel size of 0.195 mm was achieved (126). However, when compared with similar technologies, higher doses of radiation must be employed. Additionally, because of the underlying process of image reconstruction based on radiation attenuation, CT scans are not well suited for imaging regions of soft tissue surrounded by large volumes of high-density material such as bone.

Fluoroscopy also uses an X-ray source and a fluorescent receiver. High-resolution 2D radiographic images can reach ~100-μm pixel resolution (127). Here as well, there is concern about the radiation dosage the patient receives.

5.5. Ultrasound

For localization in soft tissue—compared with endoscopy, MRI, CT, and positron emission tomography (PET)—only ultrasound combines good resolution, minimal adverse health effects, high speed, safety, adequate frame rates (up to 100 frames per second) (128), and low cost (129, 130). In addition, there are several situations in which only ultrasound is adequate (24). The major drawbacks of ultrasound are related to low signal-to-noise ratio and the presence of strong wave reflectors such as bones and air pockets. These may produce artifacts in ultrasound images or shield an ultrasound signal. Furthermore, the statistical analysis of reflected sound waves in pulse-echo imaging tends to produce noise or speckle because of the low signal-to-noise ratio of ultrasonic images (129, 131). The disadvantages of ultrasonic imaging may be partially overcome through passive localization techniques, based on transmission ultrasound (132). In localization

applications, frequencies up to 3 MHz are reasonable, resulting in a resolution of ~500 μm and a penetration depth of 150–200 mm (130).

The localization of a wireless medical microrobot can be accomplished with a microrobot that acts as an emitter by carrying an ultrasound transducer onboard. A cantilever or any other mechanical structure can act as such, vibrating at its resonant frequency. The emitted signal is measured by a set of receivers placed on the surface of the patient's body. Through the use of MRI data gathered offline, localization accuracy can be greatly improved (24).

5.6. Infrared and Emitted Radiation

Using infrared (IR) radiation to track a microrobot requires that it occupies a higher temperature state than the surrounding body tissue. This is difficult to achieve because the microrobot's small volume leads to almost instantaneous thermal equilibrium with its environment. If the microrobot can maintain a higher temperature, perhaps by breaking down glucose or by carrying a hot radioactive source, then IR localization becomes possible.

PET involves the injection of a short-lived radioactive source inside the body, linked with a metabolically active molecule. As the source decays, it emits a positron, whose subsequent interaction with electrons produces detectable gamma rays. Primarily, PET is used for tumor localization (133). It is possible that the same radioactive isotopes used in PET could be incorporated into a wireless microrobot. In the specific case of brachytherapy, the radioactive seed can additionally be used for localization.

Single markers can be detected, but a minimum of three fiducial markers is necessary if both location and orientation are to be determined correctly (133). The general resolution is ~4–10 mm, although with known marker geometry, this can be improved to the submillimeter range.

6. CONCLUSIONS

Minimally invasive techniques reduce postoperative pain, hospitalization duration, patient recovery time, infection risks, and overall cost, increasing the quality of care. Microrobots can serve as a near-term goal for wireless biomedical applications, and their design will be based on the task they need to accomplish and the type of environment in which they will operate. Initially, microrobots will perform simple tasks; as technology advances, we will be able to design and fabricate more complicated devices that perform sophisticated tasks, such as targeted drug delivery and in situ biopsy sampling and characterization. Developing this technology requires that we address issues such as localization and power, always keeping in mind that microrobots will be utilized in vivo.

DISCLOSURE STATEMENT

The authors are not aware of any affiliations, memberships, funding, or financial holdings that might be perceived as affecting the objectivity of this review.

ACKNOWLEDGMENTS

This work was supported in part by the NCCR Co-Me of the Swiss National Science Foundation and by the European Commission in the framework of the FP6 NEST Adventure Project ARES and the FP7 research project NANOMA. The authors would like to thank Dr. Michael Flückiger for his contribution to Section 5.5. The authors would also like to thank Hitendra R.H. Patel, M.D., of the Department of Urology at University College London; Justus Garweg, M.D., of

the Swiss Eye Institute in Bern; Carsten Framme, M.D., of the Inselspital Bern; and Frank M. Warren, M.D., of the Division of Otolaryngology in the Department of Surgery at the University of Utah for their thoughtful comments on this work. **Figure 1*e*** reprinted with permission from the Healthwise, Incorporated, USA. Healthwise Illustrations may not be reprinted without the express permission of Healthwise. Healthwise disclaims any warranty or liability for the use of this information.

LITERATURE CITED

1. Tendick F, Sastry SS, Fearing RS, Cohn M. 1998. Applications of micromechatronics in minimally invasive surgery. *IEEE/ASME Trans. Mechatron.* 3(1):34–42
2. Dario P, Carrozza MC, Benvenuto A, Menciassi A. 2000. Micro-systems in biomedical applications. *J. Micromech. Microeng.* 10(2):235–44
3. Mack MJ. 2001. Minimally invasive and robotic surgery. *J. Am. Med. Assoc.* 285(5):568–72
4. Carrozza MC, Dario P, Jay LPS. 2003. Micromechatronics in surgery. *Trans. Inst. Meas. Control* 25(4):309–27
5. Hamdorf JM, Hall JC. 2000. Acquiring surgical skills. *Br. J. Surg.* 87:28–37
6. Joseph JV, Arya M, Patel HRH. 2005. Robotic surgery: the coming of a new era in surgical innovation. *Expert Rev. Anticancer Ther.* 5(1):7–9
7. Kassim I, Phee L, Ng WS, Gong F, Dario P, Mosse CA. 2006. Locomotion techniques for robotic colonoscopy. *IEEE Eng. Med. Biol. Mag.* 25(3):49–56
8. Menciassi A, Quirini M, Dario P. 2007. Microrobotics for future gastrointestinal endoscopy. *Minim. Invasive Ther. Allied Technol.* 16(2):91–100
9. Purcell EM. 1977. Life at low Reynolds number. *Am. J. Phys.* 45(1):3–11
10. Wautelet M. 2001. Scaling laws in the macro-, micro- and nanoworlds. *Eur. J. Phys.* 22:601–11
11. Haga Y, Esashi M. 2004. Biomedical microsystems for minimally invasive diagnosis and treatment. *Proc. IEEE* 92(1):98–114
12. Howe RD, Matsuoka Y. 1999. Robotics for surgery. *Annu. Rev. Biomed. Eng.* 1:211–40
13. Taylor RH, Stoianovici D. 2003. Medical robotics in computer-integrated surgery. *IEEE Trans. Robot. Autom.* 19(5):765–81
14. Saliterman SS. 2006. *Fundamentals of BioMEMS and Medical Microdevices*. Bellingham, WA: SPIE. 608 pp.
15. Freitas RA Jr. 2005. Nanotechnology, nanomedicine and nanosurgery. *Int. J. Surg.* 3(4):243–46
16. Patel GM, Patel GC, Patel RB, Patel JK, Patel M. 2006. Nanorobot: a versatile tool in nanomedicine. *J. Drug Target.* 14(2):63–67
17. Dong LX, Nelson BJ. 2007. Robotics in the small. Part II: Nanorobotics. *IEEE Robot. Autom. Mag.* 14(3):111–21
18. Dogangil G, Ergeneman O, Abbott JJ, Pané S, Hall H, et al. 2008. Toward targeted retinal drug delivery with wireless magnetic microrobots. *Proc. IEEE/RSJ Int. Conf. Intell. Robots Syst., Nice, Fr., Sept. 22–26*, pp. 1921–26
19. Sendoh M, Ishiyama K, Arai KI, Jojo M, Sato F, Matsuki H. 2002. Fabrication of magnetic micromachine for local hyperthermia. *IEEE Trans. Magn.* 38(5):3359–61
20. Sato F, Jojo M, Matsuki H, Sato T, Sendoh M. 2002. The operation of a magnetic micromachine for hyperthermia and its exothermic characteristic. *IEEE Trans. Magn.* 38(5):3362–64
21. Byun S, Lim J-M, Paik S-J, Lee A, Koo K, et al. 2005. Barbed micro-spikes for micro-scale biopsy. *J. Micromech. Microeng.* 15:1279–84
22. Jones AC, Milthorpe B, Averdunk H, Limaye A, Senden TJ, et al. 2004. Analysis of 3D bone ingrowth into polymer scaffolds via micro-computed tomography imaging. *Biomaterials* 25(20):4947–54
23. Ergeneman O, Dogangil G, Kummer MP, Abbott JJ, Nazeeruddin MK, Nelson BJ. 2008. A magnetically controlled wireless optical oxygen sensor for intraocular measurements. *IEEE Sens. J.* 8(1):29–37
24. Flückiger M, Nelson BJ. 2007. Ultrasound emitter localization in heterogeneous media. *Proc. IEEE Int. Conf. Eng. Med. Biol. Soc., Lyon, Fr., Aug. 23–26*, pp. 2867–70

25. Rubinstein L. 2000. *A practical nanorobot for treatment of various medical problems*. Presented at Eighth Foresight Conf. Mol. Nanotechnol., Nov. 3–5, 2000, Bethesda, Md.
26. Devlin PM. 2007. *Brachytherapy: Applications and Techniques*. Philadelphia: Lippincott Williams & Wilkins. 448 pp.
27. Andrä W, Nowak H, eds. 2007. *Magnetism in Medicine: A Handbook*. Weinheim, Germany: Wiley-VCH. 629 pp. 2nd ed.
28. Baronzio GF, Hager ED. 2006. *Hyperthermia in Cancer Treatment: A Primer*. New York: Springer
29. Zhang H, Hutmacher DW, Chollet F, Poo A-N, Burdet E. 2005. Microrobotics and MEMS-based fabrication techniques for scaffold-based tissue engineering. *Macromol. Biosci.* 5(6):477–89
30. Berger SA, Goldsmith W, Lewis ER. 1996. *Introduction to Bioengineering*. Oxford, UK: Oxford Univ. Press
31. Black J, Hastings G. 1998. *Handbook of Biomaterial Properties*. London: Chapman & Hall
32. Mathieu J-B, Beaudoin G, Martel S. 2006. Method of propulsion of a ferromagnetic core in the cardiovascular system through magnetic gradients generated by an MRI system. *IEEE Trans. Biomed. Eng.* 53(2):292–99
33. Martel S, Mathieu J-B, Felfoul O, Chanu A, Aboussouan E, et al. 2007. Automatic navigation of an untethered device in the artery of a living animal using a conventional clinical magnetic resonance imaging system. *Appl. Phys. Lett.* 90(11):114105
34. Altman P, Dittmer D. 1974. *Biology Data Book*. Bethesda, MD: Fed. Am. Soc. Exp. Biol. 2nd ed.
35. Zaaroor M, Kósa G, Peri-Eran A, Maharil I, Shoham M, Goldsher D. 2006. Morphological study of the spinal canal content for subarachnoid endoscopy. *Minim. Invasive Neurosurg.* 49(4):220–26
36. Duffner F, Schiffbauer H, Glemser D, Skalej M, Freudenstein D. 2003. Anatomy of the cerebral ventricular system for endoscopic neurosurgery: a magnetic resonance study. *Acta Neurochir.* 145(5):359–68
37. Purdy PD, Fujimoto T, Replogle RE. 2005. Percutaneous intraspinal navigation for access to the subarachnoid space: use of another natural conduit for neurosurgical procedures. *Neurosurg. Focus* 19(1):E11
38. Grady MS, Howard MA III, Molloy JA, Ritter RC, Quate EG, Gillies GT. 1989. Preliminary experimental investigation of in vivo magnetic manipulation: results and potential application in hyperthermia. *Med. Phys.* 16(2):263–72
39. Grady MS, Howard MA III, Molloy JA, Ritter RC, Quate EG, Gillies GT. 1990. Nonlinear magnetic stereotaxis: three-dimensional, in vivo remote magnetic manipulation of a small object in canine brain. *Med. Phys.* 17(3):405–15
40. McNeil RG, Ritter RC, Wang B, Lawson MA, Gillies GT, et al. 1995. Functional design features and initial performance characteristics of a magnetic-implant guidance system for stereotactic neurosurgery. *IEEE Trans. Biomed. Eng.* 42(8):793–801
41. Meeker DC, Maslen EH, Ritter RC, Creighton FM. 1996. Optimal realization of arbitrary forces in a magnetic stereotaxis system. *IEEE Trans. Magn.* 32(2):320–28
42. Molloy JA, Ritter RC, Grady MS, Howard MA III, Quate EG, Gillies GT. 1990. Experimental determination of the force required for insertion of a thermoseed into deep brain tissues. *Ann. Biomed. Eng.* 18:299–313
43. Kósa G, Shoham M, Zaaroor M. 2007. Propulsion method for swimming microrobots. *IEEE Trans. Robot.* 23(1):137–50
44. Roy S, Ferrara LA, Fleischman AJ, Benzel EC. 2006. MEMS and neurosurgery. In *Therapeutic Micro/Nano Technology*, ed. T Desai, S Bhatia, M Ferrari, pp. 95–123. New York: Springer
45. Pavlica P, Barozzi L, Menchi I. 2003. Imaging of male urethra. *Eur. Radiol.* 13(7):1583–96
46. Tunn R, DeLancey JOL, Howard D, Ashton-Miller JA, Quint LE. 2003. Anatomic variations in the levator ani muscle, endopelvic fascia, and urethra in nulliparas evaluated by magnetic resonance imaging. *Am. J. Obstet. Gynecol.* 188(1):116–21
47. Bush MB, Papa Petros PE, Barrett-Lennard BR. 1997. On the flow through the human female urethra. *J. Biomech.* 30(9):967–69
48. Turna B, Nazli O, Demiryoguran S, Mammadov R, Cal C. 2007. Percutaneous nephrolithotomy: variables that influence hemorrhage. *Urology* 69(4):603–7
49. Renner C, Rassweiler J. 1999. Treatment of renal stones by extracorporeal shock wave lithotripsy. *Nephron* 81(Suppl. 1):71–81

50. Edd J, Payen S, Rubinsky B, Stoller ML, Sitti M. 2003. Biomimetic propulsion for a swimming surgical micro-robot. *Proc. IEEE/RSJ Int. Conf. Intell. Robots Syst.*, *Las Vegas*, *Nev.*, *Oct. 27–31*, pp. 2583–88
51. Kristo B, Liao JC, Neves HP, Churchill BM, Montemagno CD, Schulam PG. 2003. Microelectromechanical systems in urology. *Urology* 61:883–87
52. Jagtap AD, Riviere CN. 2004. Applied force during vitreoretinal microsurgery with handheld instruments. *Proc. IEEE Int. Conf. Eng. Med. Biol. Soc.*, *San Francisco*, *Calif.*, *Sept. 1–5*, pp. 2771–73
53. Gupta PK, Jensen PS, de Juan E Jr. 1999. Surgical forces and tactile perception during retinal microsurgery. *Lect. Notes Comput. Sci.* 1679:1218–25
54. Theocharis IP, Alexandridou A, Tomic Z. 2007. A two-year prospective study comparing lidocaine 2% jelly versus peribulbar anaesthesia for 25G and 23G sutureless vitrectomy. *Graefe's Arch. Clin. Exp. Ophthalmol.* 245:1253–58
55. Yesin KB, Vollmers K, Nelson BJ. 2006. Modeling and control of untethered biomicrorobots in a fluidic environment using electromagnetic fields. *Int. J. Robot. Res.* 25(5–6):527–36
56. Ergeneman O, Abbott JJ, Dogangil G, Nelson BJ. 2008. Functionalizing intraocular microrobots with surface coatings. *Proc. IEEE Int. Conf. Biomed. Robot. Biomechatron.*, *Scottsdale*, *Ariz.*, *Oct. 19–22*, pp. 232–37
57. Holligan DL, Gillies GT, Dailey JP. 2003. Magnetic guidance of ferrofluidic nanoparticles in an in vitro model of intraocular retinal repair. *Nanotechnology* 14:661–66
58. Wysocki J. 1999. Dimensions of the human vestibular and tympanic scalae. *Hear. Res.* 135:39–46
59. Curthoys IS, Oman CM. 1987. Dimensions of the horizontal semicircular duct, ampulla and utricle in the human. *Acta Otolaryngol.* 103:254–61
60. Stratigouleas ED, Perry BP, King SM, Syms CA III. 2006. Complication rate of minimally invasive cochlear implantation. *Otolaryngol. Head Neck Surg.* 135:383–86
61. Parker MA, Cotanche DA. 2004. The potential use of stem cells for cochlear repair. *Audiol. Neuro-Otol.* 9:72–80
62. Flake AW. 2003. Surgery in the human fetus: the future. *J. Physiol.* 547(1):45–51
63. Berris M, Shoham M. 2006. Febotics—a marriage of fetal surgery and robotics. *Comput. Aided Surg.* 11(4):175–80
64. Jacobson SA, Epstein AH. 2003. An informal survey of power MEMS. *Int. Symp. Micro-Mech. Eng.* 12:513–19
65. DiSalvo FJ. 1999. Thermoelectric cooling and power generation. *Science* 285(5428):703–6
66. Kasap SO. 2006. *Principles of Electronic Materials and Devices*. New York: McGraw-Hill. 3rd ed.
67. Bullen RA, Arnot TC, Lakeman JB, Walsh FC. 2006. Biofuel cells and their development. *Biosens. Bioelectron.* 21:2015–45
68. Barton SC, Gallaway J, Atanassov P. 2004. Enzymatic biofuel cells for implantable and microscale devices. *Chem. Rev.* 104:4867–86
69. Morishima K, Tanaka Y, Ebara M, Shimizu T, Kikuchi A, et al. 2006. Demonstration of a bio-microactuator powered by cultured cardiomyocytes coupled to hydrogel micropillars. *Sens. Actuators B* 119(1):345–50
70. Kim J, Park J, Lee J, Yoon E, Park J, Park S. 2008. Biohybrid microsystems actuated by cardiomyocytes: microcantilever, microrobot, and micropump. *Proc. IEEE Int. Conf. Robot. Autom.*, *Pasadena*, *Calif.*, *May 19–23*, pp. 880–85
71. Xi JZ, Schmidt JJ, Montemagno CD. 2005. Self-assembled microdevices driven by muscle. *Nat. Mater.* 4(2):180–84
72. Martel S, Mohammadi M, Felfoul O, Zhao L, Pouponneau P. 2009. Flagellated magnetotactic bacteria as controlled MRI-trackable propulsion and steering systems for medical nanorobots operating in the human microvasculature. *Int. J. Robot. Res.* 28(4):571–82
73. Collins CM, Yang B, Yang QX, Smith MB. 2002. Numerical calculations of the static magnetic field in three-dimensional multi-tissue models of the human head. *Magn. Reson. Imaging* 20(5):413–24
74. Siauve N, Scorretti R, Burais N, Nicolas L, Nicolas A. 2003. Electromagnetic fields and human body: a new challenge for the electromagnetic field computation. *Int. J. Comput. Math. Electr. Electron. Eng.* 22(3):457–69
75. Popovic M, Popovic BD, Popovic Z. 2006. Electromagnetic induction. In *Fundamentals of Engineering Electromagnetics*, ed. R Bansal. Boca Raton, FL: Taylor & Francis

76. Theodoridis MP, Mollov SV. 2005. Distant energy transfer for artificial human implants. *IEEE Trans. Biomed. Eng.* 52(11):1931–38
77. International Commission on Non-Ionizing Radiation Protection (ICNIRP). 1998. Guidelines for limiting exposure to time-varying electric, magnetic, and electromagnetic fields (up to 300 GHz). *Health Phys.* 74:494–522
78. Lenaerts B, Puers R. 2007. An inductive power link for a wireless endoscope. *Biosens. Bioelectron.* 22(7):1390–95
79. Guanying M, Guozheng Y, Xiu H. 2007. Power transmission for gastrointestinal microsystems using inductive coupling. *Physiol. Meas.* 28(3):N9–18
80. Furlani EP. 2001. *Permanent Magnet and Electromechanical Devices: Materials, Analysis, and Applications*. San Diego, CA: Academic. 518 pp.
81. Abbott JJ, Ergeneman O, Kummer MP, Hirt AM, Nelson BJ. 2007. Modeling magnetic torque and force for controlled manipulation of soft-magnetic bodies. *IEEE Trans. Robot.* 23(6):1247–52
82. Nagy Z, Ergeneman O, Abbott JJ, Hutter M, Hirt AM, Nelson BJ. 2008. Modeling assembled-MEMS microrobots for wireless magnetic control. *Proc. IEEE Int. Conf. Robot. Autom., Pasadena, Calif., May 19–23*, pp. 874–79
83. White FM. 1991. *Viscous Fluid Flow*. New York: McGraw-Hill. 2nd ed.
84. Vogel S. 2003. *Comparative Biomechanics: Life's Physical World*. Princeton, NJ: Princeton Univ. Press
85. Honda T, Arai KI, Ishiyama K. 1996. Micro swimming mechanisms propelled by external magnetic fields. *IEEE Trans. Magn.* 32(5):5085–87
86. Ghosh A, Fischer P. 2009. Controlled propulsion of artificial magnetic nanostructured propellers. *Nano Lett.* 9(6):2243–45
87. Zhang L, Abbott JJ, Dong LX, Kratochvil BE, Bell DJ, Nelson BJ. 2009. Artificial bacterial flagella: fabrication and magnetic control. *Appl. Phys. Lett.* 94:064107
88. Zhang L, Abbott JJ, Dong LX, Peyer KE, Kratochvil BE, et al. 2009. Characterizing the swimming properties of artificial bacterial flagella. *Nano Lett.* 9(10):3663–67
89. Sendoh M, Ishiyama K, Arai K-I. 2003. Fabrication of magnetic actuator for use in a capsule endoscope. *IEEE Trans. Magn.* 39(5):3232–34
90. Ishiyama K, Arai KI, Sendoh M, Yamazaki A. 2003. Spiral-type micro-machine for medical applications. *J. Micromechatron.* 2(1):77–86
91. Li H, Tan J, Zhang M. 2009. Dynamics modeling and analysis of a swimming microrobot for controlled drug delivery. *IEEE Trans. Autom. Sci. Eng.* 6(2):220–27
92. Ikeuchi K, Yoshinaka K, Tomita N. 1997. Low invasive propulsion of medical devices by traction using mucus. *Wear* 209:179–83
93. Abbott JJ, Peyer KE, Cosentino Lagomarsino M, Zhang L, Dong LX, et al. 2009. How should microrobots swim? *Int. J. Robot. Res.* 28(11–12):1434–47
94. Behkam B, Sitti M. 2006. Design methodology for biomimetic propulsion of miniature swimming robots. *ASME J. Dyn. Syst. Meas. Control* 128(1):36–43
95. Kósa G, Jakab P, Jólesz F, Hata N. 2008. Swimming capsule endoscope using static and RF magnetic field of MRI for propulsion. *Proc. IEEE Int. Conf. Robot. Autom., Pasadena, Calif., May 19–23*, pp. 2922–27
96. Yu TS, Lauga E, Hosoi AE. 2006. Experimental investigations of elastic tail propulsion at low Reynolds number. *Phys. Fluids* 18:091701
97. Lauga E. 2007. Floppy swimming: viscous locomotion of actuated elastica. *Phys. Rev. E* 75:041916
98. Guo S, Sawamoto J, Pan Q. 2005. A novel type of microrobot for biomedical application. *Proc. IEEE/RSJ Int. Conf. Intell. Robots Syst., Edmonton, Can., Aug. 2–6*, pp. 1047–52
99. Sudo S, Segawa S, Honda T. 2006. Magnetic swimming mechanism in a viscous liquid. *J. Intell. Mater. Syst. Struct.* 17(8–9):729–36
100. Dreyfus R, Baudry J, Roper ML, Fermigier M, Stone HA, Bibette J. 2005. Microscopic artificial swimmers. *Nature* 437(6):862–65
101. Roper M, Dreyfus R, Baudry J, Fermigier M, Bibette J, Stone HA. 2006. On the dynamics of magnetically driven elastic filaments. *J. Fluid Mech.* 554:167–90
102. Gauger E, Stark H. 2006. Numerical study of a microscopic artificial swimmer. *Phys. Rev. E* 74:021907

103. Roper M, Dreyfus R, Baudry J, Fermigier M, Bibette J, Stone HA. 2008. Do magnetic micro-swimmers move like eukaryotic cells? *Proc. R. Soc. Lond. Ser. A* 464:877–904
104. Gillies GT, Ritter RC, Broaddus WC, Grady MS, Howard MA III, McNeil RG. 1994. Magnetic manipulation instrumentation for medical physics research. *Rev. Sci. Instrum.* 65(3):533–62
105. Stereotaxis. 2008. **http://www.stereotaxis.com**
106. Pankhurst QA, Connolly J, Jones SK, Dobson J. 2003. Applications of magnetic nanoparticles in biomedicine. *J. Phys. D* 36:R167–81
107. Kalambur VS, Han B, Hammer BE, Shield TW, Bischof JC. 2005. In vitro characterization of movement, heating and visualization of magnetic nanoparticles for biomedical applications. *Nanotechnology* 16:1221–33
108. Kuperman V. 2000. *Magnetic Resonance Imaging: Physical Principles and Applications*. San Diego, CA: Academic
109. Hinojosa FA, Martel S. 2005. Suggested shape for a first generation endovascular untethered microdevice prototype. *Proc. IEEE Int. Conf. Eng. Med. Biol. Soc.*, *Shanghai*, *China*, *Sept. 1–4*, pp. 1286–88
110. Yesin KB, Vollmers K, Nelson BJ. 2004. Guidance of magnetic intraocular microrobots by active defocused tracking. *Proc. IEEE/RSJ Int. Conf. Intell. Robots Syst.*, *Sendai*, *Jpn.*, *Sept. 28–Oct. 2*, pp. 3309–14
111. Bergeles C, Shamaei K, Abbott JJ, Nelson BJ. 2010. Single-camera focus-based localization of intraocular devices. *IEEE Trans. Biomed. Eng.* In press
112. Bergeles C, Fagogenis G, Abbott JJ, Nelson BJ. 2009. Tracking intraocular microdevices based on colorspace evaluation and statistical color/shape information. *Proc. IEEE Int. Conf. Robot. Autom.*, *Kobe*, *Japan*, *May 12–17*, pp. 3934–39
113. Northern Digital Inc. 2008. *The Aurora Electromagnetic Measurement System*. **http://www.ndigital.com/medical/aurora.php**
114. Ascension Technology Corporation. 2008. *Flock of Birds*. **http://www.ascension-tech.com/realtime/RTflockofBIRDS.php**
115. Kirsch SR, Schilling C, Brunner G. 2006. Assessment of metallic distortions of an electromagnetic tracking system. *Proc. SPIE* 6141:61410J
116. LaScalza S, Arico J, Hughes R. 2003. Effect of metal and sampling rate on accuracy of Flock of Birds electromagnetic tracking system. *J. Biomech.* 36(1):141–44
117. Hu C, Meng MQ-H, Mandal M. 2006. The calibration of 3-axis magnetic sensor array system for tracking wireless capsule endoscope. *Proc. IEEE/RSJ Int. Conf. Intell. Robots Syst.*, *Beijing*, *China*, *Oct. 9–15*, pp. 162–67
118. Hu C, Meng MQ-H, Mandal M. 2005. Efficient magnetic localization and orientation technique for capsule endoscopy. *Int. J. Inf. Acquis.* 2(1):23–36
119. Rankin SC. 2005. CT and MRI. *Surgery* 23(5):162–65
120. Schick F. 2005. Whole-body MRI at high field: technical limits and clinical potential. *Eur. Radiol.* 15(5):946–59
121. Azmi H, Schulder M. 2003. Stereotactic accuracy of a 3-Tesla magnetic resonance unit. *Stereotact. Funct. Neurosurg.* 80(1–4):140–45
122. Chinzei K, Kikinis R, Jolesz F. 1999. MR compatibility of mechatronic devices: design criteria. *Lect. Notes Comput. Sci.* 1679:1020–30
123. Felfoul O, Martel S, Beaudoin G, Mathieu J-B. 2004. Microdevice's susceptibility difference based MRI positioning system, a preliminary investigation. *Proc. IEEE Int. Conf. Eng. Med. Biol. Soc.*, *San Francisco*, *Calif.*, *Sept. 1–5*, pp. 1140–43
124. Seeram E. 2009. *Computed Tomography: Physical Principles*, *Clinical Applications*, *and Quality Control*. Philadelphia: Saunders. 560 pp. 3rd ed.
125. Fitton I, Steenbakkers RJHM, Zijp L, Duppen JC, Comans EFI, et al. 2007. Retrospective attenuation correction of PET data for radiotherapy planning using a free breathing CT. *Radiother. Oncol.* 83:42–48
126. Duryea J, Magalnick M, Alli S, Yao L, Wilson M, Goldbach-Mansky R. 2008. Semiautomated three-dimensional segmentation software to quantify carpal bone volume changes on wrist CT scans for arthritis assessment. *Med. Phys.* 35(6):2321–30

127. Antonuk LE, Jee K-W, El-Mohri Y, Maolinbay M, Nassif S, et al. 2000. Strategies to improve the signal and noise performance of active matrix, flat-panel imagers for diagnostic X-ray applications. *Med. Phys.* 27(2):289–306
128. Xu X-C, Hu C-H, Sun L, Yen J, Shung KK. 2005. High-frequency high frame rate ultrasound imaging system for small animal imaging with linear arrays. *IEEE Ultrason. Symp.* 3:1431–34
129. Wells PNT. 2000. Current status and future technical advances of ultrasonic imaging. *IEEE Eng. Med. Biol. Mag.* 19(5):14–20
130. Vilkomerson D, Lyons D. 1997. A system for ultrasonic beacon-guidance of catheters and other minimally invasive (in the original title, they write "minimally-invasive") medical devices. *IEEE Trans. Ultrason. Ferroelectr. Freq. Control* 44(2):496–504
131. Stoll J, Dupont P, Howe RD. 2002. Ultrasound-based servoing of manipulators for telesurgery. *Proc. SPIE* 4570:78–85
132. Greenleaf JF, Johnson SA, Samayoa WF, Duck FA. 1975. Algebraic reconstruction of spatial distributions of acoustic velocities in tissue from their time-of-flight profiles. *Acoust. Hologr.* 6:71–90
133. Xu T, Wong JT, Shikhaliev PM, Ducote JL, Al-Ghazi MS, Molloi S. 2006. Real-time tumor tracking using implanted positron emission markers: concept and simulation study. *Med. Phys.* 33(7):2598–609